Nanoscale

PAPER

View Article Online
View Journal | View Issue

Published on 16 November 2015. Downloaded by University of Utah on 27/01/2016 19:04:53.

Cite this: *Nanoscale*, 2015, **7**, 20042

Development and characterization of antibody reagents for detecting nanoparticles†

Supriya Ravichandran,[a] Mark A. Sullivan,[b] Linda M. Callahan,[c] Karen L. Bentley[c] and Lisa A. DeLouise*[a,d]

Received 21st July 2015,
Accepted 7th November 2015

DOI: 10.1039/c5nr04882f

www.rsc.org/nanoscale

The increasing use of nanoparticles (NPs) in technological applications and in commercial products has escalated environmental health and safety concerns. The detection of NPs in the environment and in biological systems is challenged by limitations associated with commonly used analytical techniques. In this paper we report on the development and characterization of NP binding antibodies, termed NProbes. Phage display methodology was used to discover antibodies that bind NPs dispersed in solution. We present a proof-of-concept for the generation of NProbes and their use for detecting quantum dots and titanium dioxide NPs *in vitro* and in an *ex vivo* human skin model. Continued development and refinement of NProbes to detect NPs that vary in composition, shape, size, and surface coating will comprise a powerful tool kit that can be used to advance nanotechnology research particularly in the nanotoxicology and nanotherapeutics fields.

The global total market value for nanoparticles (NPs) in biotechnology is estimated to reach $53.5B US dollars in 2017.[1] The increased formulation of NPs in therapeutics[2] and in consumer goods such as cosmetics,[3] bicycle frames, tennis rackets, skis, and other sporting goods[4] has raised human environmental health and safety (EH&S) concerns, especially for chronic low dose unintended occupational bodily exposures.[5] NP safety concerns stem from their small size and high surface area to volume ratio, which imparts unique physiochemical properties and reactivity that are not present in the bulk form.[6] When in contact with biological systems, these properties can alter tissue function[7] and lead to potential toxicity.[8,9] While metal oxide NPs such as TiO_2 and ZnO are formulated into ~70% of all sunscreens,[10] the global market for QD NPs, which are commonly used in biomedical imaging,[11] biosensing[12] and photovoltaic[13] applications, is expected to reach a value of $1.1 billion in 2016.[14]

A key route for NPs to entry the body is through skin, which is the largest organ in the body. Existing results on NP skin penetration show varying trends that are largely dependent upon the NP size and surface chemistry,[15–17] the skin model used,[18,19] the status of the skin barrier (intact or disrupted),[19,20] and the analytical techniques employed to detect the NPs.[7,16,21,22] While many studies report that for NPs to penetrate into the viable epidermis a defect is required in the stratum corneum barrier that maybe induced by tape stripping,[19] dermabrasion,[18] flexing[18,23] or UVR exposure,[20,24] however, contrasting literature reports exist.[25,26] It is important to note that the analytical techniques employed in these studies differed as would the NP detection limits which were typically not reported. For instance, it was observed based on TEM and tissue histology results that TiO_2 and ZnO NPs predominantly localize as aggregates in the stratum corneum (outer most layer of skin) but analysis using time-of-flight secondary ion mass spectrometry (TOF-SIMS) found high levels of both elemental Ti and Zn deep in the epidermal layers,[16] emphasizing the importance of considering the detection sensitivity of the analytical technique employed to detect NPs. Transmission electron microscopy (TEM) coupled with energy dispersive X-ray spectroscopy (EDS) has superior nanoscale resolution and elemental detection capability that can provide a detailed analysis of NP localization in sub-cellular regions; however, a typical tissue slice used in TEM imaging is only 70–100 nm thick.[22] Therefore, NPs present in tissue at very low levels may be missed due to sampling error. NPs may also be missed if elemental levels fall below the EDS instrument detection limit. To improve on the ability to detect NPs using TEM a colloidal silver enhancement strategy has been developed.[27] Here, colloidal silver selectively deposits onto metal/semiconducting NPs to produce larger particles that can be more easily

[a]*Department of Biomedical Engineering, University of Rochester, Rochester, New York 14642, USA. E-mail: Lisa_DeLouise@urmc.rochester.edu*
[b]*Department of Microbiology and Immunology, University of Rochester Medical Centre, Rochester, New York 14642, USA*
[c]*Department of Pathology and Laboratory Medicine, University of Rochester Medical Centre, 601 Elmwood Avenue, Box 626, Rochester, New York 14642, USA*
[d]*Department of Dermatology, University of Rochester Medical Centre, Rochester, New York 14642, USA*

†Electronic supplementary information (ESI) available: Figures and detailed methods of various techniques used. See DOI: 10.1039/c5nr04882f

This journal is © The Royal Society of Chemistry 2015

Published on 16 November 2015. Downloaded by University of Utah on 27/01/2016 19:04:53.

identified and distinguished from spurious tissue dark features. In previous work, we routinely observed higher QD presence in the viable epidermis using this procedure compared to histological analysis using fluorescence microscopy.[20,22] To achieve a more quantitative measure of NP presence, *in vivo* elemental organ analysis is typically performed on digested tissue samples using atomic absorption spectroscopy (AAS) or inductively coupled plasma mass spectrometry (ICP-MS). This approach provides a sensitive means to quantify the systemic transport of NPs. However, the tissue digestion process obfuscates the ability to distinguish transport of intact NPs from soluble ion transport.[28] For some elements detection may be masked by interference from abundant trace metals or from endogenous elements such as carbon.[16] The isotopic enrichment method outlined by Gulson *et al.*[29] can be used as a means to eliminate uncertainty pertaining to background levels of trace elements; however, this method is prohibitively expensive and impractical for routine NP studies. Confocal and fluorescence microscopy are also common techniques used to visualize the presence of fluorescent NPs in tissues and while they allow for background noise reduction, the presence of NPs at low levels may still be obscured by tissue autofluorescence.[22]

In order to unify published data on the topic of "Nanomaterials: environmental and health effects", an action plan has been recommended in a recent review.[30] In this plan, one of the recommendation states that "an integral part of the harmonization of experimental methods is conclusive and feasible analytics; therefore, the development of appropriate and inexpensive analytical methods should be a part of funding programs".[30] To this end and with a goal to better understand NP skin penetration, we have undertaken an effort to develop a simple technique that can provide information on both the NP presence and form[31] in the environment and in a biological milieu, which can be used in conjunction with existing quantitative techniques. Here we present our initial efforts to develop antibody reagents that bind NPs (NProbes) using phage display technology. Phage display is a common method used to discover protein or peptide binders to a wide variety of targets. Typically, the nucleotide sequence encoding a peptide is fused to the phage coat protein gene allowing the peptide to be displayed on the phage exterior.[32] A library of phage displaying unique peptides is created and an affinity based selection technique (bio-panning) is used to discover binders. Phage display technology has been successfully used to isolate peptides recognizing inorganic metals,[33–36] metal oxides[37–39] and semiconductors.[40] In this work we use an antibody phage library which offers more diversity in terms of binding surface to discover more selective and high affinity reagents based on shape as well as composition. While very little is currently known about the ability of the immune system to recognize NPs,[41,42] NP immunogenicity is not a requirement for enrichment of antibody binders using *in vitro* display technology as we are working with a preexisting library of human antibodies and do not rely on an *in vivo* B cell immune response to occur.

In this work NProbes were selected from a phage library consisting of $\sim 2 \times 10^9$ unique single chain variable fragment (scFv) antibodies each displayed monovalently on the minor pIII coat protein of M13 filamentous phage. This library has been used by us previously to generate scFvs against proteins[43] and cell surface antigens.[44] A key difference from our prior work is that here we have developed protocols to conduct biopanning on NPs dispersed in solution rather than the standard method of immobilizing the target onto a substrate.[45] In this work the scFv antibodies were engineered with a peptide FLAG tag (DYKDDDDKL) to enable secondary detection/amplification of NP presence in tissue sections using standard immunohistochemistry (IHC) staining with an enzymatic reporter. Herein, we demonstrate a proof-of-concept for NProbe generation and their use for detecting QDs and TiO_2 NPs using *in vitro* assays and *ex vivo* human skin models.

Results and discussion

Selection of binders to QDs and TiO_2 using phage display

For NProbe discovery we used glutathione-coated (GSH) QDs (CdSe/ZnS core/shell) and TiO_2 NPs (Evonik/Degussa, 80% anatase and 20% rutile crystal, ~21 nm primary particle size). We selected the GSH-QDs for their superior stability to resist agglomeration in water and buffer systems compared to other commonly used water soluble coatings such as dihydrolipoic acid (DHLA) (ESI Fig. S1†).[46] The hydrodynamic diameter and polydispersity of the GSH-QDs measured in water using dynamic light scattering (DLS) were 14.1 ± 2.5 nm and 0.33 ± 0.06, respectively and they were negatively charged (−22.82 mV) as determined from zeta potential measurements (pH = 5.3–5.6). The Evonik TiO_2 was selected because of its wide use in commercial skin care products.[47] TiO_2 NPs dispersed in water form aggregates that range from ~100 nm to ~1.5 μm when visualized under TEM (ESI Fig. S1†). NProbes to GSH-QDs and TiO_2 NPs were isolated using affinity-based biopanning which involves mixing the target NPs with the phage library. The GSH-QDs (400 μl, 100 nM) and the TiO_2 NPs (400 μl, 0.5 mg ml^{-1}) were diluted in tris-buffered saline (TBS) and mixed with the phage library (100 μl, $\sim 10^{12}$ phage per mL in TBS plus 0.5% casein) with gentle agitation. In the TBS buffer system the GSH-QDs exhibit a much lower tendency to agglomerate than the TiO_2 as seen in TEM images (ESI Fig. S1†). The hydrodynamic diameter and polydispersity of the GSH-QDs in TBS was found to be 25.2 ± 1.54 nm and 0.40 ± 0.03, respectively and they were negatively charged similar to the GSH-QDs in water. For GSH-QD panning the phage input library was pre-centrifuged (Optima TLX ultracentrifuge, Beckman Coulter) at 116 000*g* (65 000 rpm) to pellet phage agglomerates. After incubation for 2 h at room temperature, the NP/phage mixtures were centrifuged to pellet the NPs with bound phage. The GSH-QD/phage mixture was centrifuged at 83 000*g* (55 000 rpm) for 10 min and the TiO_2/phage mixture was centrifuged at 1300*g* (4000 rpm) for 5 min. After removing unbound phage in the supernatant, the pellets

Published on 16 November 2015. Downloaded by University of Utah on 27/01/2016 19:04:53.

were resuspended in TBS containing 0.05% Tween-20 (TBST). Wash cycles of centrifugation and re-suspension in TBST were repeated 5 times, following which the pellet was washed once in deionized water. After washing, the bound phages were eluted from the NPs using 0.1 M glycine (pH 2.2) and neutralized using 2 M Tris base. The titer of the eluted phage was quantified by transduction of ampicillin-resistant TG1 *Escherichia coli* host cells and the resulting colonies were counted. A phage pool for the next round of enrichment was generated by transduction of 20–100% of the previous round eluate. After overnight incubation, the pooled transductants were grown at 37 °C, infected with VCS M13 helper phage, and grown overnight at 30 °C. Phage stocks were prepared for the next round of panning by polyethylene glycol (PEG) precipitation. Typically, 4 rounds of panning were necessary to enrich for specific binders to NPs, after which a BstNI fingerprinting analysis was performed. The presence of identical restriction enzyme patterns among the tested clones was taken as evidence of specific enrichment as we have previously shown.[44] The BstNI digests of 12 randomly selected clones following four rounds of NP panning typically found pattern repeats indicating 17–25% clonal abundance (ESI Fig. S2†). This was increased to >50% after five rounds of panning. Phage clones from the enriched populations, termed GSH43ϕ and Ti49ϕ, were selected for testing. It is important to note however, that the most abundant phage clones may not be strongest binders or exhibit the highest selectivity. On-going studies seek to characterize the binding affinity and selectivity of additional clones identified. The amino acid sequences of the scFvs for the two phage clones selected for study are given in ESI Table 1.† It is interesting to point out that the CDR regions for both the GSH43 and the Ti49 scFvs are comprised of a high percentage of polar uncharged amino acids (serine and asparagine); 30% and 32%, respectively. Surprisingly, the CDR regions lack a preponderance of cysteines (<3%) and histidines (<1%) which typically are enriched in metal ion binding peptides.[48] This suggests an alternative mechanism is important for scFv antibodies binding to NPs. The GSH43ϕ and Ti49ϕ phage clones and their respective purified scFv antibodies were freshly prepared and used for *in vitro* verification of target binding and cross reactivity testing to similar and dissimilar materials which we discuss next.

Verification of NP binding *in vitro* using phage clones

In vitro assays were conducted to quantify the binding of the GSH43ϕ and Ti49ϕ clones to their respective NP targets and to test their cross reactivity binding to other NPs and to negative control phage clones including interleukin-12 (IL-12ϕ), lactoferrin (LFϕ), human GRP78 (BiPϕ) and a 15 amino acid (PVSP (ps)SQKLKRKAEEDPE) peptide (Npepϕ). First, we used a phage centrifugation titer assay to assess binding. Here, the NPs were mixed with the GSH43ϕ, Ti49ϕ or IL-12ϕ clones for 2 h at room temperature. After removal of unbound phage by centrifugation, the pellet was washed 5 times with TBST buffer, after which the phages were eluted and the titers quantified as discussed above. Results for the GSH43ϕ and Ti49ϕ clones consistently showed a 10-fold and 100-fold increase in binding to their target NP, respectively relative to the IL-12ϕ negative control (ESI Fig. S3†). The lower enrichment value observed for the GSH43ϕ likely results from the precipitation of unbound phage during the ultracentrifugation step causing higher background counts in the colony assay despite our efforts to pre-centrifuge the phage to clear aggregates. These values are nonetheless are in accordance with an 8-fold enrichment that was reported for isolating peptides against solid ZnO substrates using phage display.[38] To show that the phage clones exhibit sequence specific binding we exchanged the light chain of GSH43ϕ clone with the light chain of IL-12ϕ and the hybrid phage was tested for binding to the GSH-QDs. This manipulation reduced the hybrid phage binding to the GSH-QDs by a factor of 4. To further verify phage binding we conducted TEM analysis. The GSH-QDs were mixed separately with the GSH43ϕ clone and the IL-12ϕ negative clone. Similarly, the TiO_2 NPs were mixed separately with the Ti49ϕ clone and the IL-12ϕ negative clone. After a 2 h incubation at room temperature the four samples were washed to remove unbound phages using the centrifugation procedure described above. The pellets were re-suspended in TBS buffer and prepared for TEM analysis. Results (Fig. 1 and ESI Fig. S4†) show evidence for Ti49ϕ bound to TiO_2 NPs (black arrows, Fig. 1a), whereas the IL-12ϕ negative clone did not (Fig. 1b). TEM results also show the GSH43ϕ bound to the GSH-QDs causing phage clustering (Fig. 1c), whereas the IL-12ϕ negative phage did not (Fig. 1d). The apparent association of the GSH-QD with the major coat protein (PVIII) is a likely artifact of the harsh ultracentrifugation process which may cause QDs to dislodge and become trapped in the phage pellet that is resuspended on the TEM grid. This does not happen in the control phage due to lack of GSH-QD binding in the solution phase.

To test for potential cross-reactivity binding to similar and dissimilar NPs that vary in core composition and surface coating we conducted phage titer assays using the centrifugation method and a custom plate titer assay. Results from the centrifugation titer assay (Fig. 2 and ESI Fig. S5†) indicate that the Ti49ϕ clone binds to the TiO_2 (Evonik P25) and to TiO_2 NPs from a secondary vendor (Sigma Aldrich Inc., #677469) whereas negligible binding to Au-powder (<10 μm particle size Sigma Aldrich Inc., #326585), citrate coated 20 nm Au NPs (Sigma Aldrich Inc., #753610) and carboxylated multi-walled carbon nanotubes (CNT-MWSusp-100, NanoLab, Inc.) is seen. Additionally, the Ti49ϕ bound other TiO_2 NPs including TiO_2-anatase crystalline form (TiO_2-A, 32 nm size, Alfa Aesar) and TiO_2-rutile crystalline form (TiO_2-R, ~200 nm size, DuPont) demonstrating universal recognition of all forms of TiO_2 NPs (Fig. 3). Highest binding was observed to TiO_2-R potentially attributing to its larger particle sizes compared to the other forms (ESI Fig. S6†). The centrifugation titer assay was also used to test the cross reactivity binding of the GSH43ϕ clone to the carboxylated CNTs and the citrated 20 nm Au NPs which showed negligible binding similar to IL-12ϕ negative control (Fig. 4 and ESI Fig. S5†).

 This journal is © The Royal Society of Chemistry 2015

Published on 16 November 2015. Downloaded by University of Utah on 27/01/2016 19:04:53.

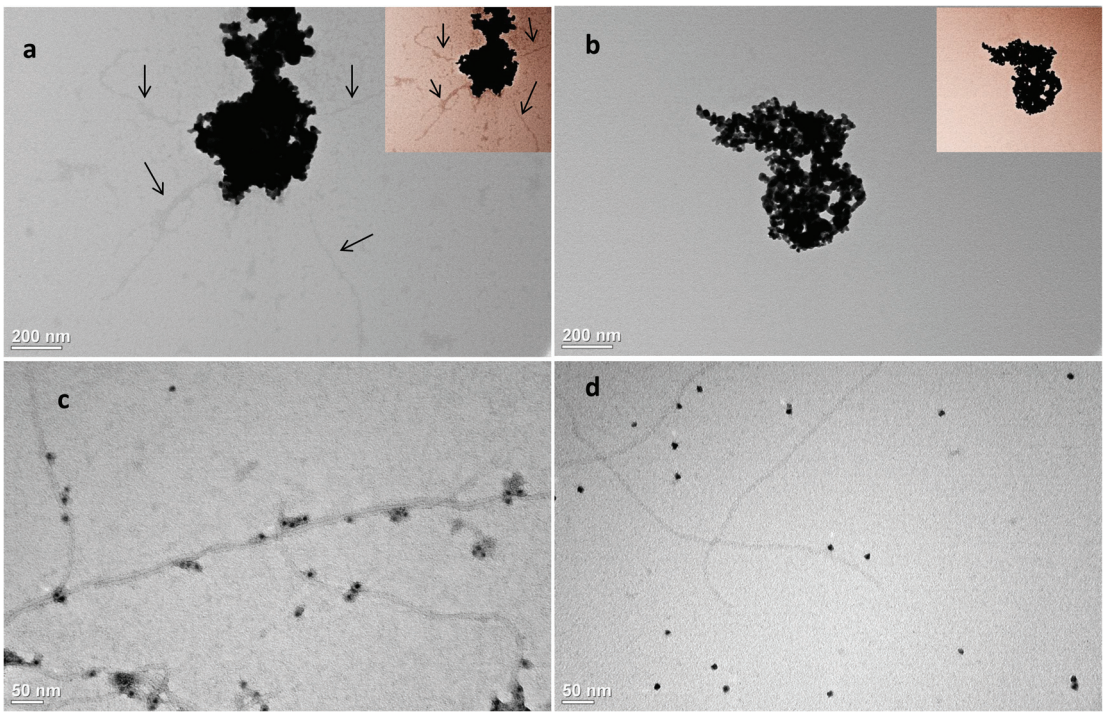

Fig. 1 TEM studies of phage binding to respective NP. TEM images showing (a) Ti49ϕ (black arrows) binding TiO_2 NPs whereas (b) there is no evidence for IL-12ϕ (negative control) to bind TiO_2 NPs. Scale bar = 200 nm. Inset are image enhanced to highlight the phage. (c) GSH43ϕ exhibit strong association and clustering with GSH-QDs whereas and (d) the negative control IL-12ϕ show no affinity for the GSH-QD which appear highly dispersed. Scale bar = 50 nm.

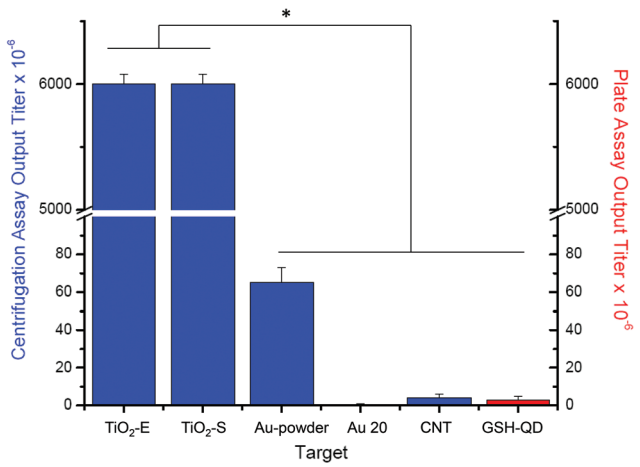

Fig. 2 Results from centrifugation and plate titer assays to examine Ti49ϕ phage cross reactivity binding to similar and dissimilar materials. Results from the centrifugation titer assay (blue bars) indicates that Ti49ϕ binds Evonik TiO_2 NPs (TiO_2-E) and TiO_2 NPs from a secondary vendor (Sigma, TiO_2-S) but minimal binding is observed to dissimilar materials including Au-powder particles (Sigma), 20 nm Au (Sigma, Au20), and CNTs (NanoLab, Inc.). Using the plate titer assay the Ti49ϕ bound the GSH-QDs at background levels. Colonies on the agar plates were counted manually and values plotted on the *y*-axis. Error bars are the (number of colonies)$^{1/2}$. Values are statistically significant as observed using a Student's *t* test ($p < 0.001$).

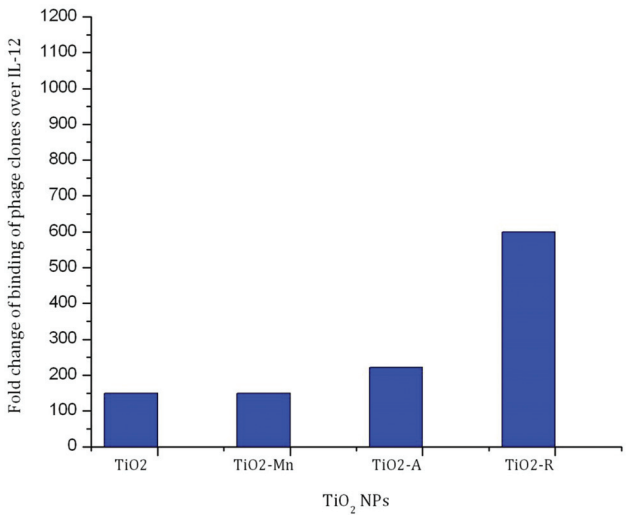

Fig. 3 Binding of Ti49ϕ to TiO_2NPs. Binding of Ti49ϕ to different TiO_2 NPs varying in composition and source. (A) Using a centrifugation titer assay, Ti49ϕ was found to bind TiO_2-Mn (Sigma Aldrich Inc.) similar to TiO_2NPs (Evonik, P25), bound TiO_2-R higher (by 3-fold), and bound TiO_2-A by ~1.5-fold more than the other TiO_2 NPs.

Published on 16 November 2015. Downloaded by University of Utah on 27/01/2016 19:04:53.

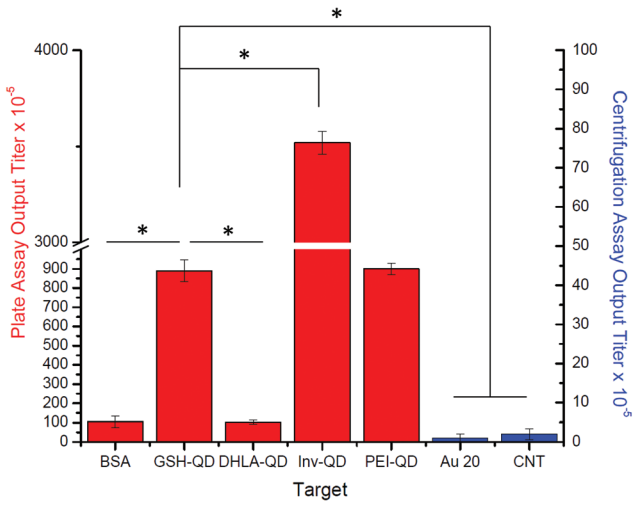

Fig. 4 Results from centrifugation and plate titer assays to examine GSH43ϕ phage cross reactivity binding to similar and dissimilar materials. Plate titer assay results (red bars) indicate that the GSH43ϕ clone exhibits strong binding to negative charged GSH-QDs (~9-fold over the BSA-only, p = 0.0035, no QD control sample), to negative charged Invitrogen (p = 0.0005) and positive charged PEI-QDs (p = 0.8, not significant). However, minimal binding is seen to negative charged DHLA-QDs (p = 0.0028) and also to dissimilar materials including 20 nm Au NPs and CNTs (p = 0.002) determined by the centrifugation titer assay (blue bars). Colonies on the agar plates were counted manually and values plotted on the y-axis. Error bars are the (number of colonies)$^{1/2}$. Statistical analysis was done using Student's t-test and values were considered significant if $p < 0.05$. All samples were compared to binding of GSH43ϕ to GSH-QDs to measure significance.

To evaluate the cross reactivity binding of the GSH43ϕ clone to QDs with similar core composition (ZnS/CdSe core/shell) but different coating chemistries we developed a plate titer assay to minimize background signal that results from inadvertent precipitation of unbound phage using ultracentrifugation separation. Following a literature protocol,[49] high binding 96 well plates were treated with 2% BSA prior to depositing the QDs. The QDs (50 µl of a 50 nM solution in sodium bicarbonate buffer) were added to the wells and allowed to incubated overnight at 4 °C with gentle agitation. The deposition and adherence of QDs before and after the multiple washing steps (7 TBST washes, 1 water wash) was confirmed using a handheld UVR light source (ESI Fig. S7†). Prior to conducting cross reactivity studies we first validated the binding of the GSH43ϕ to immobilized GSH-QDs relative to empty vector phage containing the his6 and flag tags. No binding was observed for the empty vector phage, whereas GSH43ϕ displayed a 200-fold more binding to GSH-QDs over phage control (ESI Fig. S8†). Moreover, the GSH43ϕ bound the immobilized GSH-QDs in a dose dependent manor (ESI Fig. S8†). These results provided confidence that the plate titer assay could be used to examine NP cross reactivity binding. Results from the plate titer assay (Fig. 4) show that GSH43ϕ (upon elution with glycine pH 2.2) binds to GSH-QD (25.2 nm and negatively charged), Invitrogen QDs (Inv-QD, Invitrogen ITK™ 565-QDs, 10 nm and negatively charged), and PEI-QD (23 nm and positively charged)[46] but minimal binding to the DHLA-QD (14 nm and negatively charged) is observed. These data suggest that QD binding in the phage format is not specific to the GSH coating or to surface charge. Moreover, using the plate titer assay (Fig. 2 and ESI Fig. S9†) we found that Ti49ϕ did not bind GSH-QDs confirming the absence of cross-reactivity of the Ti49ϕ clone to GSH-QDs. To confirm these results we next examined the scFv binding to similar and dissimilar materials which is the intended NProbe format.

Verification of NP binding *in vitro* using scFvs

To examine the scFv binding characteristics we generated soluble His-tagged scFv protein that was affinity purified and characterized by SDS-PAGE gels to verify the purity was >95% (ESI Fig. S10†). To examine scFv binding to similar and dissimilar materials we first conducted dot blot assays to test the binding of the GSH43-scFv, the Ti49-scFv and the BiP-scFv (negative control) to GSH-QDs, Au NPs and CNTs that were spotted on a nitrocellulose membrane (Fig. 5(i)–(iii), left column). Similar to the phage binding studies (Fig. 4), the GSH43-scFvs showed high specific binding to the GSH-QDs indicated by the dark chemiluminescent spot formed (Fig. 5(i), right column). GSH43-scFv did not bind Au NPs (pink spot, center) or CNTs (black spot, right). The negative control BiP-scFv (Fig. 5(ii)) and the Ti49-scFv (Fig. 5(iii)) did not bind the GSH-QDs, the Au NPs or the CNTs. To test the GSH43-scFv binding to similar core materials but with different coating ligands we spotted GSH-QDs, Inv-QDs, DHLA-QDs and PEI-QDs on a nitrocellulose membrane (Fig. 5(iv), left column). Chemiluminescence detection of scFv binding using HRP (Fig. 5(iv), right column), shows that GSH43-scFvs bind GSH-QDs and DHLA-QDs, but not Inv-QDs and PEI-QDs. The negative control NT3-scFvs (Fig. 5(v)) showed only a faint background staining to all these QDs. The lack of GSH43-scFv binding to the PEI-QDs is in contrast to the strong binding observed in the phage format (Fig. 4). We attribute this to non-specific binding of the positive PEI-QDs to the M13 phages which carry a high negative surface charge.[50] The lack of GSH43-scFv binding to the negative charged Inv-QD is also in contrast to the phage format results (Fig. 4). We attribute this to differences in binding affinity, as from dot blot concentration studies we did observe strong binding of the GSH-scFv to the Inv-QD with increasing GSH-scFv concentration (5–20 µg mL^{-1}) with a continued absence of binding to PEI-QDs (ESI Fig. S11†). The binding of GSH43-scFv to DLHA-QDs appears much stronger than in the plate titer assay (Fig. 4) which may suggest the QD coating affects adherence to BSA coated plate. Over all, these results suggest that the GSH-scFv recognizes QDs with a similar core/shell composition but with different binding affinity which is also likely modulated the composition and liability of the surface ligand coating. Binding of GSH43-scFv to GSH-QDs was further confirmed using dynamic light scattering (DLS) with the BiP-scFv as the negative control. Here, the GSH-QDs were mixed with the scFvs at room temp for 2 h and ultra-centrifuged washed as

 This journal is © The Royal Society of Chemistry 2015

Published on 16 November 2015. Downloaded by University of Utah on 27/01/2016 19:04:53.

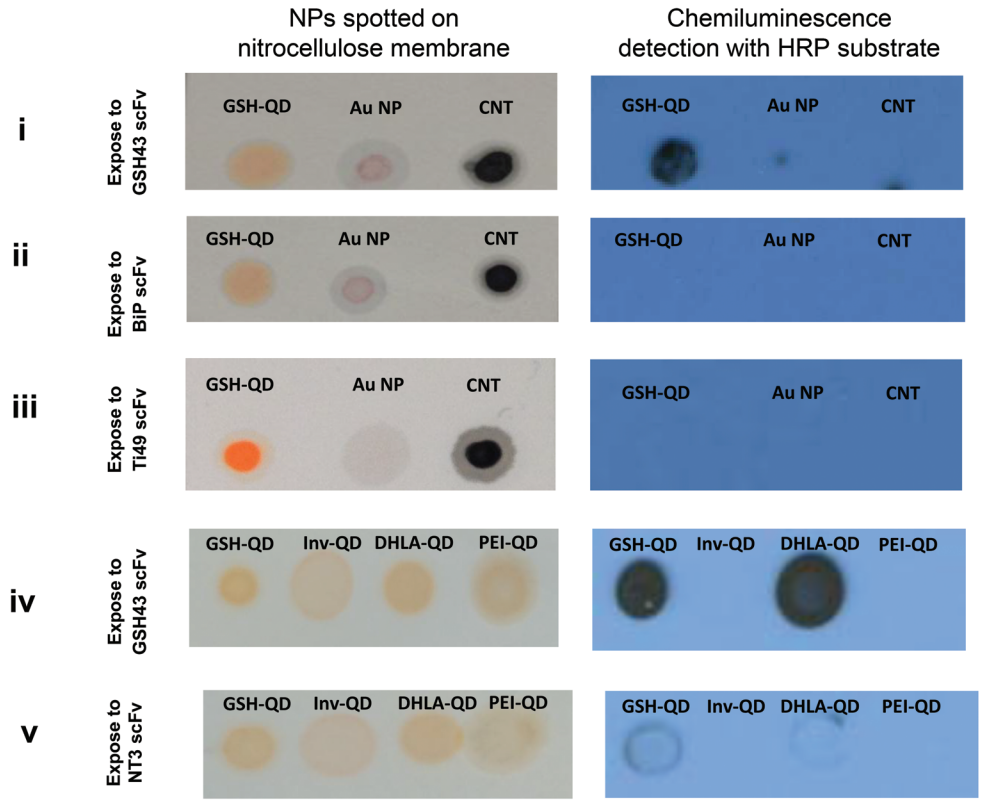

Fig. 5 Dot blots investigating scFv binding to similar and dissimilar materials. For dissimilar materials, spots on a nitrocellulose membrane (left column) showing GSH-QDs (orange), Au NPs (pink) and CNTs (black) spots. Chemiluminescence detection of scFv binding with HRP (right column). Results show that (i) GSH43-scFv (5 μg mL^{-1}) binds GSH-QDs but not Au NPs and CNTs, (ii) negative control BiP-scFv (5 μg mL^{-1}) and (iii) Ti49-scFv (5 μg mL^{-1}) do not bind any of the NPs. For similar materials, GSH-QDs, Invitrogen ITK™ 565-QDs (Inv-QDs), DHLA-QDs, and PEI QDs were spotted on a nitrocellulose membrane (left column). Upon chemiluminescence detection of scFv binding using HRP (right column), results show that (iv) GSH43-scFvs bind GSH-QDs and DHLA-QDs at 5 μg mL^{-1}, but not Inv-QDs and PEI-QDs whereas (v) NT3 negative control scFvs show faint background staining at the same concentration.

discussed above. GSH-QDs in TBS buffer alone were also taken through the ultra-centrifugation wash and re-suspension steps for comparison. The hydrodynamic diameter of the GSH-QDs with bound GSH43-scFvs (~651 nm) was ~1.5-fold larger than that of BiP-associated GSH-QDs and ~2.5-fold GSH-QDs in TBS with statistical significance (ESI Fig. S12†). This data suggests that GSH-QDs bind to the GSH43-scFv despite their tendency to agglomerate in TBST. As further proof we conducted Image Stream flow cytometry measurement using anti-FLAG coated agarose beads. Beads coated with GSH43-scFv show intense QD fluorescence signal relative to beads exposed to GSH-QDs only, which showed no fluorescence signal. Only weak background fluorescence was detected following exposure of GSH-QDs to beads coated with negative control BiP-scFv (ESI Fig. S13†). We did not test the binding of the Ti49-scFv to TiO_2 NPs by dot-blot analysis as the presence of the NPs on the nitrocellulose membrane could not be verified by color. Hence, to confirm Ti49-scFv binding we dried the TiO_2 NPs onto a glass slide and used confocal microscopy to quantify the presence of fluorescein isothiocyanate (FITC)-conjugated anti-FLAG reporter. Images (Fig. 6(i)) were captured under bright-field and fluorescence. A control slide without TiO_2 NPs showed no background staining (ESI Fig. S14†). ImageJ (NIH) was used for analysis of line profiles of three regions of interest (ROIs) and the results averaged. Although a slight background signal was detected for Npep-scFv on TiO_2 the quantification clearly shows a significant difference in the level of Ti49-scFv binding to TiO_2 NPs compared to negative control ($p < 0.05$, student's unpaired *t*-test, Fig. 6(ii)).

Validation of scFvs to detect NPs in a biological milieu

The main motivation for developing NProbe reagents is to facilitate the detection of NPs in biological systems in their particulate form. Existing studies of NP skin penetration have highlighted the need to consider the detection limits of the analytical techniques used as well as the assay protocol in drawing definitive conclusions about the NP skin penetration.[16,22] Having developed and characterized NProbe binding reagents to TiO_2 and QD NPs using *in vitro* assays, we next sought to test their ability to detect NPs in a biological milieu. First, we immobilized GSH-QDs on a glass slide coated with collagen, which is a key component of skin, and tested binding to GSH43-scFvs relative to a negative control (NPep-scFv) using confocal microscopy. We observed strong specific

Published on 16 November 2015. Downloaded by University of Utah on 27/01/2016 19:04:53.

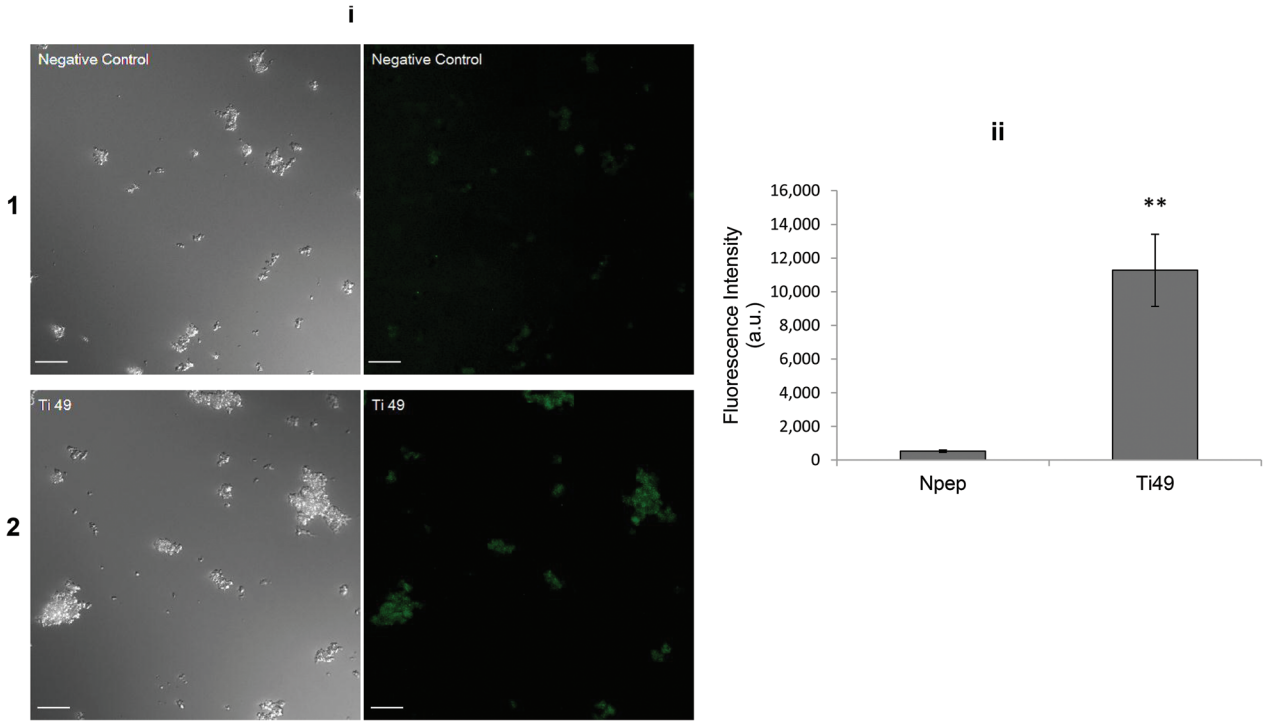

Fig. 6 Brightfield and confocal images investigating the binding of Ti49-scFvs to TiO_2NPs immobilized on a glass slide using FITC-conjugated anti-FLAG secondary antibody detection. (i) Representative images of negative control Npep-scFv showing minimal binding to TiO_2 NPs (row 1), whereas Ti49-scFvs shows strong binding to TiO_2NPs (row 2). Scale bar = 20 μm. (ii) Quantitative analysis of the integrated fluorescence intensity shows significant difference in the Ti49-scFv treated sample compared to negative control Npep-scFv. Data shown is average of three ROIs from the images. Error bars indicate SEM. $^{**}p$ = 0.0075 using student's unpaired *t*-test.

GSH43-scFvs binding to the GSH-QDs as indicated by the Pearson's co-localization coefficient of 0.65 (ESI Fig. S15†). GSH43-scFvs did not bind collagen films without containing QDs (data not shown). Next, we tested the ability of the scFv to detect NPs in fresh *ex vivo* human skin. NPs were topically applied to fresh *ex vivo* human using established protocols.[19] Following NP skin exposure the tissue was cryo-sectioned for immuno-histochemical (IHC) analysis using NProbes and a secondary anti-FLAG reporter conjugated to an alkaline phosphatase (AP). Skin slices were pre-treated with levamisole (5 μM) to eliminate endogenous phosphatase activity. Fig. 7 shows bright-field and fluorescent images of a skin section following a 24 h application GSH-QDs to the stratum corneum and a control sample (no QD exposure). The control sample shows negligible AP staining (Fig. 7a) indicating the absence of non-specific GSH43-scFv binding to the skin sections. In contrast, the skin sample exposed to GSH-QDs shows numerous punctate areas of strong AP staining in bright-field (Fig. 7b). Observation of this skin section under fluorescence imaging shows a dense cluster of QDs (Fig. 7c) that co-localizes with AP staining (blue arrows, Fig. 7b inset). However, based on fluorescence imaging (Fig. 7c) the detection of GSH-QD presence in skin is suggested to be far less than that suggested by AP staining. Using ImageJ software the fluorescence image can be threshold enhanced (Fig. 7d) which reveals many more potential instances of QDs in the skin tissue; but as previously noted[22] it is difficult to unambiguously distinguish the QDs from tissue autofluorescence artifacts. Results from AP staining (Fig. 7b) however, clearly demonstrate the utility of NProbes to overcome this challenge. The AP staining identifies many areas that co-localize with high fluorescence (black arrows, Fig. 7b and d). Additionally, we observed regions with strong AP staining with corresponding regions that do not show presence of QD fluorescence (red arrows, Fig. 7b and d). This suggests that NProbes can identify QDs whose fluorescence cannot be detected over autofluorescence background. To validate that the areas of strong AP staining do indeed contain QDs we used laser capture micro-dissection (LCM) microscopy to isolate portions of the tissue sample by catapulting them into AdhesiveCap™ microfuge tubes, which were then assayed for elemental cadmium (Cd) using atomic absorption spectroscopy (AAS). Initial studies were conducted on a skin sample with a high QD presence introduced by dermal injection to ensure Cd levels exceeded the AAS detection limit of detection (LOD) equal to 7 pg ml^{-1}. The control skin sample (no QDs) again showed no discernable AP staining and no visible fluorescence QD signal (exposure time: 800 ms) (ESI Fig. S16†). In contrast, strong AP staining is seen under bright-field in the dermis where GSH-QDs were injected as shown in Fig. 8a with the corresponding QD fluorescence before dissection shown in Fig. 8b. The portion of the skin marked for dissection is enclosed in the blue dotted area

 This journal is © The Royal Society of Chemistry 2015

Published on 16 November 2015. Downloaded by University of Utah on 27/01/2016 19:04:53.

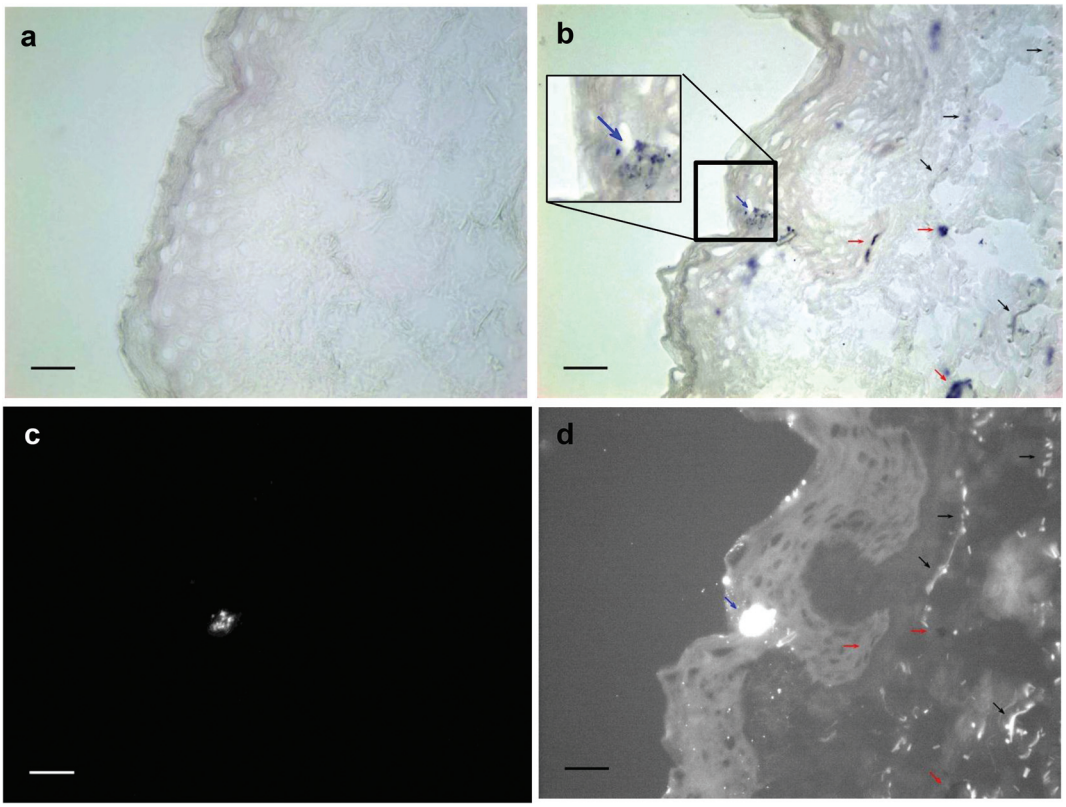

Fig. 7 QD detection in *ex vivo* human skin using GSH43-scFv. Skin slices were pretreated with levamisole to reduce endogenous phosphatase activity. (a) Control skin sample without GSH-QD exposure showing an absence of AP staining indicating a lack of GSH43-scFv non-specific binding to skin. (b) Brightfield image of skin sample exposed to GSH-QDs for 24 h showing numerous areas with strong AP staining (black, blue, and red arrows). Inset shows an area of high AP staining (blue arrow) in the epidermis that correlates with high QD presence as seen under (c) fluorescence imaging, exposure 1.642 s. (d) Applying a threshold to enhance the fluorescent signal shows that some of the areas with strong AP staining (black arrows) co-localize with QD fluorescence, whereas other areas (red arrows) indicate potential presence of QDs that are not visible under the fluorescence exposure conditions used. This suggests the ability of GSH43-scFv to detect the presence of QDs that may otherwise being undetectable in skin. This was confirmed with LCM studies. Scale bar = 50 μm.

(Fig. 8c). The portion remaining after catapult is shown in Fig. 8. AAS analysis of the tissue areas where strong QD fluorescence was co-localized with AP staining was performed to confirm the presence of Cd. Results indicated detection of 214 ng mL^{-1} of Cd.

Having demonstrated the ability of the LCM/AAS techniques to detect QD presence in the positive control sample, we proceeded to use this methodology to confirm the presence QDs in epidermal regions that exhibit strong AP staining following a topical QD application on tape stripped skin (ESI Fig. S17†). Initial measurements of individual ROIs in tissue sections showed levels of Cd < LOD using AAS. However by combining six ROIs with strong AP staining we measured 108 pg mL^{-1} Cd, which is ~100 times above the LOD indicating the presence of QDs in these regions. The Cd level measured from six random ROI collected and combined from the control sample (no QD) was 8.5 pg mL^{-1}, which is near the instrument LOD (7 pg ml^{-1}) and may indicate the presence of endogenous Cd derived dietary sources which is more readily detected in the liver.[15,24] In addition, we collected and combined six ROIs with strong AP staining that lacked discernible QD signal under fluorescence imaging. AAS analysis measured 18 pg mL^{-1} Cd, which is above the instrument LOD and ~10 times higher than the endogenous Cd measured in the skin of the control (no QDs). These results demonstrate a proof-of-principle that NProbes can enable the detection of QDs (strong AP staining in bright field) present at low levels using simple IHC techniques.

We further sought to demonstrate the utility of NProbes by examining the penetration of nonfluorescent TiO_2 NPs through the human skin barrier using the Ti49-scFvs. The TiO_2 NPs (Evonik) were applied to intact skin in water and we also examined a TiO_2 containing commercial sunscreen (Eucerin SPF15). Results for both consistently show strong AP staining confined mainly to the upper layers of the stratum corneum (Fig. 9a) relative to the control (no TiO_2 NPs) which did not show AP staining (Fig. 9b). In some samples, we occasionally observed areas with mild punctate staining beneath the stratum corneum (Fig. 9a, blue arrows) suggesting that TiO_2 NPs may have penetrated the stratum corneum barrier. Attempts to confirm the presence of TiO_2 NPs in tissue using AAS proved however, unsuccessful due to difficulties in dissolving TiO_2 for elemental analysis and a poor AAS detec-

Published on 16 November 2015. Downloaded by University of Utah on 27/01/2016 19:04:53.

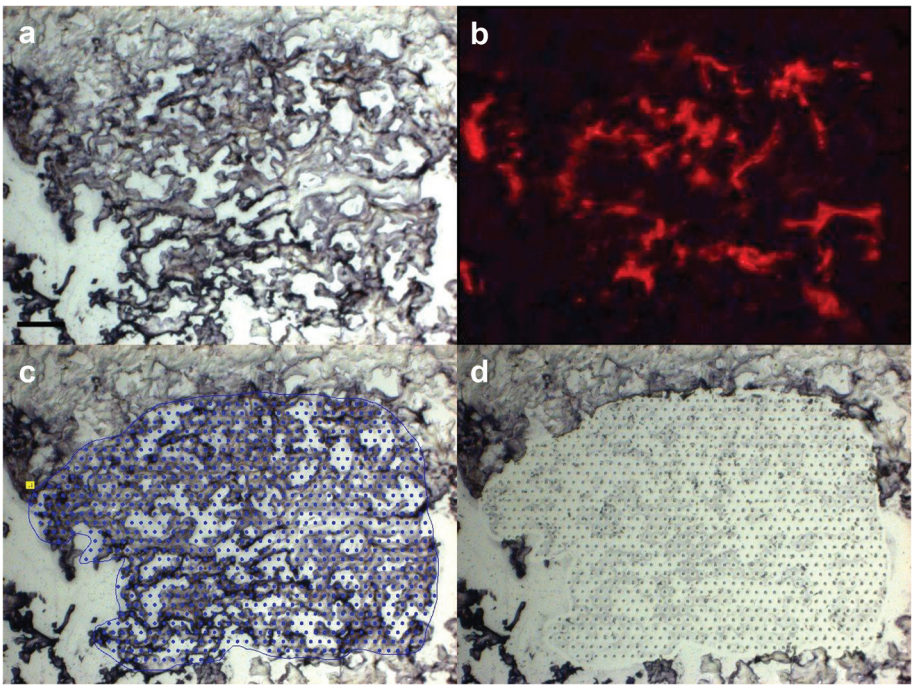

Fig. 8 LCM imaging microscopy to confirm presence of GSH-QDs in areas of high AP staining. Representative skin sample containing QDs injected showing (a) dark bluish-purple staining indicating binding of GSH43-scFvs detected by AP. (b) Fluorescence image of skin sample before dissection showing QD presence. (c) Portions of stained areas were marked for cut and captured onto adhesive tube caps using LCM, and processed for AAS. (d) The portion of skin remaining after capture. Scale bar = 50 μm.

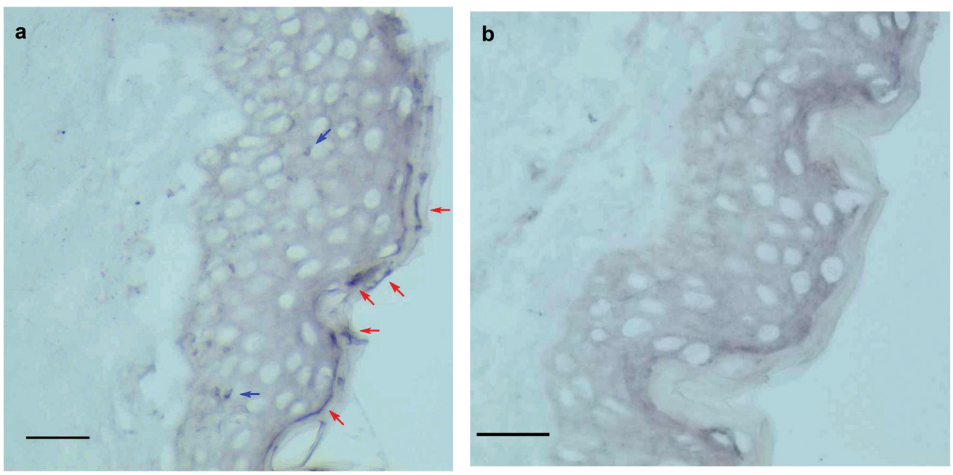

Fig. 9 Detection of TiO_2 using Ti49-scFv in human skin *ex vivo*. Representative images of (a) TiO_2 applied on epidermis of intact skin, red arrows indicates AP staining due to binding of Ti49-scFv to TiO_2 NPs. Blue arrows indicate AP staining, which could potentially be TiO_2 particles penetrated through skin to the dermis. (b) Control sample with no TiO_2 applied and upon exposure to Ti49-scFvs, no non-specific binding (no AP staining) was observed. Scale bar = 50 μm.

tion sensitivity for Ti ions. Therefore, we attempted to examine the epidermal regions exhibiting light blue staining for the presence of TiO_2 particles using SEM. First, regions of dark staining in a control sample (TiO_2 applied directly to dermis for 24 h) were analyzed to visualize the morphology of TiO_2 NPs in the tissue milieu (ESI Fig. S18†). In this control tissue sample individual TiO_2 NPs could be readily discerned as part of larger aggregates. However, SEM analysis of several experimental skin samples exhibiting light blue staining in the epidermis and dermis were less conclusive as individual particles in the TiO_2 aggregates were harder to discern (ESI Fig. S19†). We were also unable to detect Ti ions in these regions using

 This journal is © The Royal Society of Chemistry 2015

Published on 16 November 2015. Downloaded by University of Utah on 27/01/2016 19:04:53.

SEM/EDX. This is not unexpected however; as we estimate our TiO_2 EDX detection limit to be 0.5–5 μg cm^{-2} which likely far exceeds the TiO_2 NP presence in these skin samples. Nevertheless, we are able to conclude that our results are consistent with the preponderance of recent literature investigating of TiO_2 NP skin penetration using different animal models,[17,20,51,52] that significant penetration of beyond the stratum corneum is likely hindered by the high tendency of TiO_2 NPs to agglomerate.

Conclusions

In summary, using phage display technology we have discovered and characterized for the first time scFv antibody reagents that bind GSH-QDs and TiO_2 NPs and we have further demonstrated a proof-of-principle that these NProbe reagents can be used to simply detect NPs in skin using the standard immuno-histochemical technique. This work is unique in our approach to bio-pan on NPs dispersed in solution. Typically phage display requires the target to be immobilized onto a solid support by chemical coupling[53] or non-covalent adsorption to a hydrophobic surface.[54] A previous study[49] reported isolation of peptides using phage display that bind QDs immobilized on protein (gelatin)-coated polystyrene plates. However, when we immobilized QDs on gelatin and performed enrichments, only clones that bound gelatin were found. This phenomenon has been previously reported, where often off-target unrelated clones are enriched that bind to other components in the screening system rather than the target itself.[55] In fact, phage binding to components other than the target such as the solid phase (plastic, plates), substances used for blocking (BSA, milk) and capturing agents may predominate during rounds of bio-panning.[55] We also observed this in our efforts to pan on QDs immobilized to BSA coated plate which only generated binders to BSA. Hence, our solution phase panning approach helps to minimize occurrences of false positives and favors identification of clones recognizing the NPs dispersed in solution. It is clear however, from the data presented that the phage are panned against NP aggregates and that shape must be a key recognition element as the expected metal binding amino acids are not predominant in the antibody CDR regions. Moreover, the enrichments values (10 to 100 fold) are less than expected for typical phage panning on proteins bound to a plate (>1000 fold). A plausible explanation is that the scFv "recognition epitope" varies dynamically in the panning process due to agglomeration. Future studies are planned to investigate this.

In this proof-of-concept study we demonstrated the utility of scFv antibodies to detect GSH-QDs and TiO_2 NPs in both *in vitro* and in the *ex vivo* human skin model. The scFvs isolated did not bind dissimilar materials tested, namely Au NPs, Au powder or CNTs. Several controls were included to validate binding including the use of random scFvs selected from the library and 'no-NP' controls in all experiments. The data presented herein for non-fluorescent TiO_2 detection validates the preponderance of current literature, which reports TiO_2 NPs agglomerates predominantly localize in the upper layers of the stratum corneum. However, we do observed instances of mild AP staining below the stratum corneum both for skin application of TiO_2 NPs from water and from a TiO_2 containing commercial sunscreen (Eucerin SPF 15). In these regions SEM studies confirmed the presence of structures that morphologically resemble TiO_2 aggregates suggesting possible presence in viable skin layers. However, efforts to detect the elemental Ti (EDX) proved inconclusive. In the QD studies we were able to confirm that instances of AP straining in the epidermis with and without a co-localized fluorescent signal did contain elemental Cd. Hence, it is likely that the instances of mild AP staining in the epidermis on TiO_2 treated skin (albeit less frequent that in QD treated skin) do indeed contain NPs. It is not unexpected that some TiO_2 NPs could penetrate through defects in the stratum corneum barrier.

In summary, we have discovered scFv antibodies that can bind to NPs and we show the advantage of using enzymatic reporting to amplify the detection NPs in skin. Our methodology can be further exploited to develop NProbes for binding other NP types thereby providing an expansive tool kit that can complement other techniques to further our understanding of NP interactions in biological systems from a toxicology and therapeutic perspective. NProbes antibodies will be particularly advantageous for detecting non-fluorescent NPs using cost-effective and common imaging techniques. Therefore, we expect that NProbes can be advanced and used in conjunction with conventional techniques to overall improve NP detection abilities in tissues and other biological systems. In future studies we will seek to discover the mechanisms of NP scFv binding and how binding affinity and selectivity relate to NP agglomeration. In addition we will construct scFv-Fc fusion proteins which will provide more stable reagents that will be easier for investigators to work with.

Materials and methods

Quantum dot synthesis

Commercially available CdSe/ZnS core/shell QDs capped with octadecylamine (ODA) (NN-Labs, 5.8 nm core diameter and 620 nm emission wavelength) were purchased. Previously described[46] ligand exchange methods were used to prepare water-soluble GSH-QDs. Briefly, ODA-QDs (300 μL) were precipitated by addition of methanol : acetone (1 : 1) and separated by centrifugation at 14 000 rpm for 5 min. The ODA-QDs were resuspended in 300 μL tetrahydrofuran (THF). 30 mg GSH (Cat. number 3541, Calbiochem) was added to 1 mL methanol and adjusted to pH 11.0 with tetramethylammonium hydroxide pentahydrate powder. The ODA-QD THF solution was slowly added to the GSH-methanol solution while stirring, at room temperature in a 4 mL glass vial (VWR) immersed in a mineral oil bath (light white oil, Sigma-Aldrich Inc.) and the mixture was stirred at 60 °C for 2 h on a hotplate/stirrer (VWR). The GSH-QDs were then precipitated with the addition

Published on 16 November 2015. Downloaded by University of Utah on 27/01/2016 19:04:53.

of excess ether (1–2 mL) and centrifuged at 14 000 rpm for 5 min. The supernatant was discarded and GSH-QDs were resuspended in 300 μL 0.01 N NaOH and dialysed using a 5 kD molecular weight cutoff DispoDialyzer filter (Harvard Apparatus Inc.) against excess water (50 mL water, changed once) for 48 h.

scFv preparation

Preparation of the scFv protein from positive binders and negative controls was performed by removing the M13 gene III fragment of the display vector by digestion of the plasmid with SalI and XhoI, followed by re-ligation of the compatible ends. This manipulation also appends a hexa-histidine tag to the carboxy terminus of the scFv to permit affinity purification of the protein on an immobilized Ni^{2+} resin. The scFvs also contain a FLAG epitope (DYKDDDDKL) at the amino terminus of the light chain domain to enable secondary detection. After removal of gene III fragment, the scFvs were prepared by growth of the cultures in medium with limiting inorganic phosphate to induce expression from the *phoA* promoter. The cell pellets were lysed with BugBuster™ (Novagen) and the His-tagged scFvs were purified on Ni^{2+} magnetic beads using a Thermo KingFisher instrument to automate bead washing. The scFvs were eluted from the washed beads using PBS containing 300 mM imidazole, and stored at 4 °C. Prior to using scFvs in experiments, SDS-PAGE gel was used to confirm presence of scFvs in the sample. The gel was stained with Coomasie Blue (Simply Blue, Invitrogen) and photographed. The approximate concentration of the scFv purified was determined by measuring the absorbance at 280 nm and normalizing it with the reading for pure imidazole used during the above-mentioned elution step.

SEM imaging

TiO_2 detection limit quantification on the Zeiss Supra 40VP Field Emission SEM was done by preparing coverslips with 50 μL each of 1, 0.1 and 0.01 mg mL^{-1} TiO_2 in water pipetted onto an area of 1 cm^2. EDX spectra were obtained for each of the samples were a discernable peak for Ti was observed for 1 (50 μg cm^{-2} TiO_2) and 0.1 mg mL^{-1} (5 μg cm^{-2} TiO_2) samples but not for 0.01 mg mL^{-1} (0.5 μg cm^{-2} TiO_2) sample.

Image stream flow cytometry

Anti-FLAG antibody coated commercially available beads (Sigma Aldrich Inc.) were used to coat GSH43 and BiP scFvs passively overnight at 4 °C. Beads were collected and centrifuged to remove excess scFvs. The beads were blocked in 2% BSA in TBS for 1 h at room temperature. GSH-QDs at a concentration of 50 nM were added to samples containing scFv-coated beads and to a sample of uncoated beads. QDs were not added to the 'beads only' control. QDs were allowed to incubate with the beads for 2 h at room temperature with gentle agitation, after which the beads were washed in TBS with repeated centrifugation and re-suspension. The beads were finally re-suspended in 60 μL TBS and analyzed using Image Stream under brightfield and fluorescence using appropriate lasers for QDs. Images were analyzed using IDEAS Application software (version 6.0).

Human skin processing and NP application

Fresh viable human skin from adult donors was obtained following a mammoplasty or abdominoplasty within hours of surgery. Skin samples were approved for usage by the University of Rochester Research Subjects Review Board (RSRB). The skin was washed thrice with 1× phosphate-buffered saline (PBS) and treated with fungizone (Invitrogen) to remove any microbial contamination. Skin was then processed to remove fat and thin the dermis for easy handling. The samples were placed on gauze in a sterile petri-dish filled with media (5–8 mL) to keep the skin viable. GSH-QDs and TiO_2 NPs were applied on to skin in quantities lesser (0.01 mg cm^{-2}) than those routinely used for cosmetic testing (0.05 mg cm^{-2}) by pipetting and spreading them evenly on the epidermal side of the skin. Skin samples were tape stripped (Scotch 3M 3750 clear packing tape, USA) ten times prior to application of GSH-QDs. Each piece of fresh tape was pressed firmly onto the epidermal surface of the skin and removed. GSH-QDs were also injected (50 μL in 100 μL deionized water) using an insulin needle (skin rested with stratum corneum facing upwards) from epidermis to dermis as a positive control sample. Skin samples were placed in the sterile hood for 24 h, after which excess NPs will be wiped off the skin surface using 1× PBS. All the samples were stored at −80 °C until processing for histology.

IHC

Frozen skin was mounted using TEK OCT compound, after which they were sliced (5 μm thickness) on to microscope slides using a cryostat (Thermo Scientific). The epidermis and the dermis were sectioned simultaneously to prevent accidental transfer of NPs to the blade. The slides were fixed in methanol (−20 °C, 10 min) prior to the experiment and dipped in water (Ultrapure™ water, Invitrogen) to remove excess OCT. The slides were washed twice with 1× TBS to wash off excess methanol and a hydrophobic pen was used to create a water-repellent barrier to keep reagents localized on the tissue specimen. The slides were blocked with normal mouse serum for 30 min at room temperature, after which GSH43-scFvs were added to the slides diluted in BSA (10 μg mL^{-1}) and allowed to incubate overnight at 4 °C in a humidified chamber. The slides were washed thrice with 1× TBST and incubated with anti-FLAG antibody conjugated to alkaline phosphate (AP) (Sigma-Aldrich Inc.) for 1 h at room temperature. After washing away excess antibodies, the slides were incubated with BCIP/NBT (KPL) substrate for AP containing 5 mM levamisole (Vector laboratories Inc., CA) for 30 min at room temperature. Levamisole is an endogenous AP inhibitor that enables visualization of AP staining due to the binding of scFv-anti-FLAG AP-tagged antibody alone. Excess substrate solution was washed away with DI water and mowiol (Fluka, #81381, Sigma Aldrich Inc., synthesized in-house) was used as a mounting medium for imaging. The samples were analyzed

 This journal is © The Royal Society of Chemistry 2015

Published on 16 November 2015. Downloaded by University of Utah on 27/01/2016 19:04:53.

under a fluorescent microscope (Nikon Eclipse E800 with a Spot RTS Camera) at 40× magnification. Images were captured using brightfield and appropriate fluorescence filters, and analyzed using ImageJ (NIH).

Conflict of interest

The authors declare no competing financial interests.

Acknowledgements

The authors thank Michael Tiberio (URMC) for help with protein purification. The authors acknowledge Paivi Jordan (Confocal Microscopy Core, URMC) for her help with the confocal microscope. The authors thank Bob Gelein (URMC) for his help with AAS. The authors acknowledge funding from The Centers for Disease Control and Prevention (1R21OH009970).

References

1 http://www.bccresearch.com/market-research/biotechnology/nanoparticles-biotechnology-drug-development-delivery-bio113a.html.
2 M. A. Maurer-Jones, K. C. Bantz, S. A. Love, B. J. Marquis and C. L. Haynes, *Nanomedicine*, 2009, **4**, 219–241.
3 C. O. Robichaud, A. E. Uyar, M. R. Darby, L. G. Zucker and M. R. Wiesner, *Environ. Sci. Technol.*, 2009, **43**, 4227–4233.
4 M. Endo, T. Hayashi, Y. A. Kim, M. Terrones and M. S. Dresselhaus, *Philos. Transact. A, Math. Phys. Eng. Sci.*, 2004, **362**, 2223–2238.
5 Woodrow Wilson Intl. Center for Scholars. News release: nanotech-enabled consumer products top the 1000 mark [Internet]. August 25, 2009. Available from: available at: http://www.nanotechproject.org.
6 S. K. Misra, D. Mohn, T. J. Brunner, W. J. Stark, S. E. Philip, I. Roy, V. Salih, J. C. Knowles and A. R. Boccaccini, *Biomaterials*, 2008, **29**, 1750–1761.
7 A. Elder, S. Vidyasagar and L. DeLouise, *Wiley Interdiscip. Rev.: Nanomed. Nanobiotechnol.*, 2009, **1**, 434–450.
8 P. V. AshaRani, G. Low Kah Mun, M. P. Hande and S. Valiyaveettil, *ACS Nano*, 2009, **3**, 279–290.
9 C. Y. Jin, B. S. Zhu, X. F. Wang and Q. H. Lu, *Chem. Res. Toxicol.*, 2008, **21**, 1871–1877.
10 T. Faunce, K. Murray, H. Nasu and D. Bowman, *Nanoethics*, 2008, **2**, 231–240.
11 F. A. Esteve-Turrillas and A. Abad-Fuentes, *Biosens. Bioelectron.*, 2013, **41**, 12–29.
12 Y. Zhang, Q. Zeng, Y. Sun, X. Liu, L. Tu, X. Kong, W. J. Buma and H. Zhang, *Biosens. Bioelectron.*, 2010, **26**, 149–154.
13 P. V. Kamat, *J. Phys. Chem. Lett.*, 2013, **4**, 908–918.
14 Wellesley, Quantum Dots: Global Market Growth and Future Commercial Prospects, Report NAN027D, April 2014.
15 N. V. Gopee, D. W. Roberts, P. Webb, C. R. Cozart, P. H. Siitonen, J. R. Latendresse, A. R. Warbitton, W. W. Yu, V. L. Colvin, N. J. Walker and P. C. Howard, *Toxicol. Sci.*, 2009, **111**, 37–48.
16 N. A. Monteiro-Riviere, K. Wiench, R. Landsiedel, S. Schulte, A. O. Inman and J. E. Riviere, *Toxicol. Sci.*, 2011, **123**, 264–280.
17 J. P. Ryman-Rasmussen, J. E. Riviere and N. A. Monteiro-Riviere, *Toxicol. Sci.*, 2006, **91**, 159–165.
18 N. A. Monteiro-Riviere and L. W. Zhang, in *Nanomaterials: Risks and Benefits*, 2009.
19 S. Ravichandran, L. J. Mortensen and L. A. DeLouise, *Nanotoxicology*, 2011, **5**, 675–686.
20 L. J. Mortensen, G. Oberdorster, A. P. Pentland and L. A. DeLouise, *Nano Lett.*, 2008, **8**, 2779–2787.
21 R. Alvarez-Román, A. Naik, Y. N. Kalia, R. H. Guy and H. Fessi, *J. Controlled Release*, 2004, **99**, 53–62.
22 L. J. Mortensen, S. Ravichandran, H. Zheng and L. A. DeLouise, *J. Biomed. Nanotechnol.*, 2010, **6**, 596–604.
23 J. G. Rouse, J. Yang, J. P. Ryman-Rasmussen, A. R. Barron and N. A. Monteiro-Riviere, *Nano Lett.*, 2007, **7**, 155–160.
24 L. J. Mortensen, S. Jatana, R. Gelein, A. De Benedetto, K. L. De Mesy Bentley, L. A. Beck, A. Elder and L. A. Delouise, *Nanotoxicology*, 2013, **7**, 1386–1398.
25 F. F. Larese, F. D'Agostin, M. Crosera, G. Adami, N. Renzi, M. Bovenzi and G. Maina, *Toxicology*, 2009, **255**, 33–37.
26 F. L. Filon, M. Crosera, G. Adami, M. Bovenzi, F. Rossi and G. Maina, *Nanotoxicology*, 2011, **5**, 493–501.
27 L. Y. Chou, H. C. Fischer, S. D. Perrault and W. C. Chan, *Anal. Chem.*, 2009, **81**, 4560–4565.
28 L. A. DeLouise, *J. Invest. Dermatol.*, 2012, **132**, 964–975.
29 B. Gulson, M. McCall, M. Korsch, L. Gomez, P. Casey, Y. Oytam, A. Taylor, M. McCulloch, J. Trotter, L. Kinsley and G. Greenoak, *Toxicol. Sci.*, 2010, **118**, 140–149.
30 H. F. Krug, *Angew. Chem., Int. Ed.*, 2014, **53**, 12304–12319.
31 C. Szakal, S. M. Roberts, P. Westerhoff, A. Bartholomaeus, N. Buck, I. Illuminato, R. Canady and M. Rogers, *ACS Nano*, 2014, **8**, 3128–3135.
32 W. G. Willats, *Plant Mol. Biol.*, 2002, **50**, 837–854.
33 R. R. Naik, S. J. Stringer, G. Agarwal, S. E. Jones and M. O. Stone, *Nat. Mater.*, 2002, **1**, 169–172.
34 S. R. Whaley, D. S. English, E. L. Hu, P. F. Barbara and A. M. Belcher, *Nature*, 2000, **405**, 665–668.
35 H. Watanabe, T. Nakanishi, M. Umetsu and I. Kumagai, *J. Biol. Chem.*, 2008, **283**, 36031–36038.
36 T. Hattori, M. Umetsu, T. Nakanishi, S. Sawai, S. Kikuchi, R. Asano and I. Kumagai, *Bioconjugate Chem.*, 2012, **23**, 1934–1944.
37 P. Golec, J. Karczewska-Golec, M. Los and G. Wegrzyn, *J. Nanopart. Res.*, 2012, **14**, 1218.
38 D. Rothenstein, B. Claasen, B. Omiecienski, P. Lammel and J. Bill, *J. Am. Chem. Soc.*, 2012, **134**, 12547–12556.
39 T. Hattori, M. Umetsu, T. Nakanishi, T. Togashi, N. Yokoo, H. Abe, S. Ohara, T. Adschiri and I. Kumagai, *J. Biol. Chem.*, 2010, **285**, 7784–7793.

Published on 16 November 2015. Downloaded by University of Utah on 27/01/2016 19:04:53.

40 A. Artzy Schnirman, E. Zahavi, H. Yeger, R. Rosenfeld, I. Benhar, Y. Reiter and U. Sivan, *Nano Lett.*, 2006, **6**, 1870–1874.
41 B. X. Chen, S. R. Wilson, M. Das, D. J. Coughlin and B. F. Erlanger, *Proc. Natl. Acad. Sci. U. S. A.*, 1998, **95**, 10809–10813.
42 D. Izhaky and I. Pecht, *Proc. Natl. Acad. Sci. U. S. A.*, 1998, **95**, 11509–11510.
43 P. Denny, F. K. Hagen, M. Hardt, L. Liao, W. Yan, M. Arellanno, S. Bassilian, G. S. Bedi, P. Boontheung, D. Cociorva, C. M. Delahunty, T. Denny, J. Dunsmore, K. F. Faull, J. Gilligan, M. Gonzalez-Begne, F. Halgand, S. C. Hall, X. Han, B. Henson, J. Hewel, S. Hu, S. Jeffrey, J. Jiang, J. A. Loo, R. R. Ogorzalek Loo, D. Malamud, J. E. Melvin, O. Miroshnychenko, M. Navazesh, R. Niles, S. K. Park, A. Prakobphol, P. Ramachandran, M. Richert, S. Robinson, M. Sondej, P. Souda, M. A. Sullivan, J. Takashima, S. Than, J. Wang, J. P. Whitelegge, H. E. Witkowska, L. Wolinsky, Y. Xie, T. Xu, W. Yu, J. Ytterberg, D. T. Wong, J. R. Yates, 3rd and S. J. Fisher, *J. Proteome Res.*, 2008, **7**, 1994–2006.
44 C. G. Haidaris, J. Malone, L. A. Sherrill, J. M. Bliss, A. A. Gaspari, R. A. Insel and M. A. Sullivan, *J. Immunol. Methods*, 2001, **257**, 185–202.
45 H. R. Hoogenboom, A. P. de Bruine, S. E. Hufton, R. M. Hoet, J. W. Arends and R. C. Roovers, *Immunotechnology*, 1998, **4**, 1–20.
46 H. Zheng, L. J. Mortensen and L. A. DeLouise, *J. Biomed. Nanotechnol.*, 2013, **9**, 382–392.
47 A. Weir, P. Westerhoff, L. Fabricius, K. Hristovski and N. von Goetz, *Environ. Sci. Technol.*, 2012, **46**, 2242–2250.
48 M. Mejare and L. Bulow, *Trends Biotechnol.*, 2001, **19**, 67–73.
49 S. Mardyani and W. C. W. Chan, *J. Mater. Chem.*, 2009, **19**, 6321–6323.
50 J. A. Lamboy, J. A. Arter, K. A. Knopp, D. Der, C. M. Overstreet, E. F. Palermo, H. Urakami, T. B. Yu, O. Tezgel, G. N. Tew, Z. Guan, K. Kuroda and G. A. Weiss, *J. Am. Chem. Soc.*, 2009, **131**, 16454–16460.
51 A. O. Gamer, E. Leibold and B. van Ravenzwaay, *Toxicol. In Vitro*, 2006, **20**, 301–307.
52 N. Sadrieh, A. M. Wokovich, N. V. Gopee, J. Zheng, D. Haines, D. Parmiter, P. H. Siitonen, C. R. Cozart, A. K. Patri, S. E. McNeil, P. C. Howard, W. H. Doub and L. F. Buhse, *Toxicol. Sci.*, 2010, **115**, 156–166.
53 S. Bass, R. Greene and J. A. Wells, *Proteins*, 1990, **8**, 309–314.
54 G. P. Smith, *Science*, 1985, **228**, 1315–1317.
55 M. Vodnik, U. Zager, B. Strukelj and M. Lunder, *Molecules*, 2011, **16**, 790–817.

 This journal is © The Royal Society of Chemistry 2015

Electronic Supplementary Material (ESI) for Nanoscale.
This journal is © The Royal Society of Chemistry 2015

Development and characterization of antibody reagents for detecting nanoparticles

Authors: Supriya Ravichandran[1], Mark A. Sullivan[2], Linda M. Callahan[3], Karen L. Bentley[3], Lisa A. DeLouise[1,4]

SUPPLEMENTARY FIGURES

[1]Department of Biomedical Engineering, University of Rochester, Rochester, New York 14642, USA.
[2]Department of Microbiology and Immunology, University of Rochester Medical Centre, Rochester, New York 14642, USA.
[3] Department of Pathology and Laboratory Medicine, University of Rochester Medical Centre, 601 Elmwood Avenue, Box 626, Rochester, New York 14642,
[4]Department of Dermatology, University of Rochester Medical Centre, Rochester, New York 14642, USA.
*email: Lisa_DeLouise@urmc.rochester.edu

Supplementary Table 1

a

Light Chain

CLONE	CDR1	CDR2	CDR3
GSH43	LPVLTQPPSASGSPGQRVTISCSGS **SSNIGSNTVN** WYQQLPGTAPKLLIY **SNNQRPS** GVPDRFSGSKSGTSASLAISGLRSEDEADYYCAA **WDDSLNG** WVFGGGTKLTVLG		
Ti49	SSELTQDPAVSVALGQTVRITC **QGDSLRSYYAS** WYQQKPGQAPVLVIY **GKNNRPS** GIPDRFSGSSSGNTASLTITGAQAEDEAEYYCYS **RDRSGNR** VIFGGGTKVTVLG		

b

Heavy Chain

CLONE	CDR1	CDR2	CDR3
GSH43	QVQLQQSGAEVKKPGASVKVSCKASGYTFN **THGFS** WVRQAPGQGLEWMGW **ISASNGNTKYPQNLQG** RVTMTVDTFTTTAYLELRSLRSDDTAVYYCVR **DRTDYYVPGTFDPLYGPFDY** WGQGTLVTVSS		
Ti49	QVQLESGPGLVKPSETLSLACTVSGGSIT **SSSYYWG** WIRQPPGKGLEWIG **SMSYRGTTYYNPSLES** RAIISADTAKNQFSLNLNSVTAADTAVYYCAR **WHCSSSMCYDLDY** WGPGTLVTVSS		

Supplementary Table 1: Amino acid sequences of **(a)** light and **(b)** heavy chain of GSH43 and Ti49 clones. The CDRs in each sequence are in bold typeface and underlined.

Supplementary Figure S1

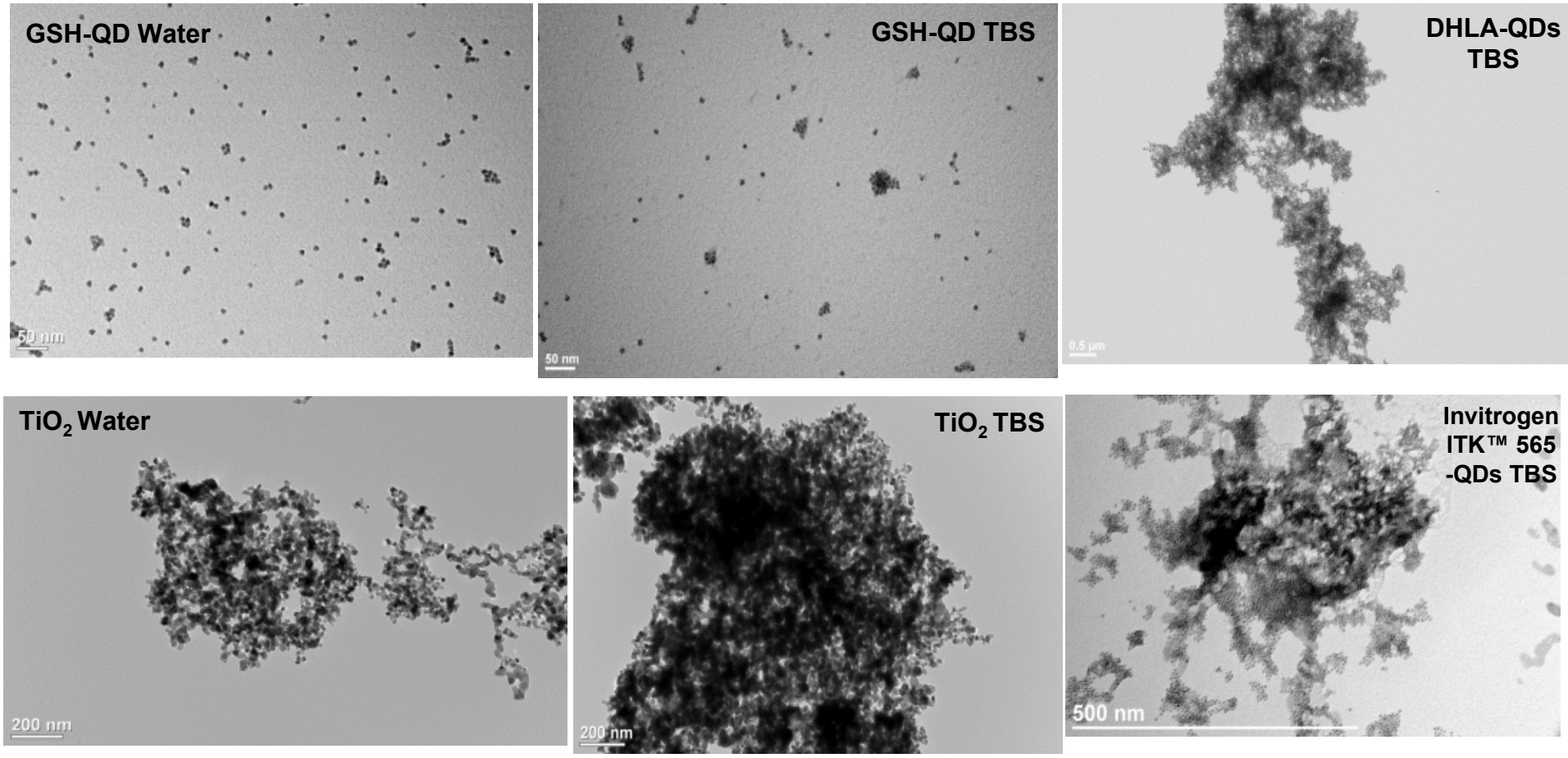

Supplementary Figure S1: TEM images of different NPs in water and TBS. GSH-QDs in water and TBS showing superior stability (Scale bar=50 nm) compared to TiO2 (Scale bar=200 nm) exhibiting agglomeration. DHLA-QDs and Invitrogen ITK™ 565-QDs in TBS showing agglomeration. Scale bar=500 nm.

Supplementary Figure S2

a

GSH-QD

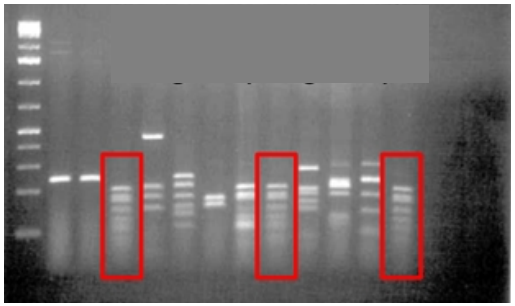

b

TiO_2 NP

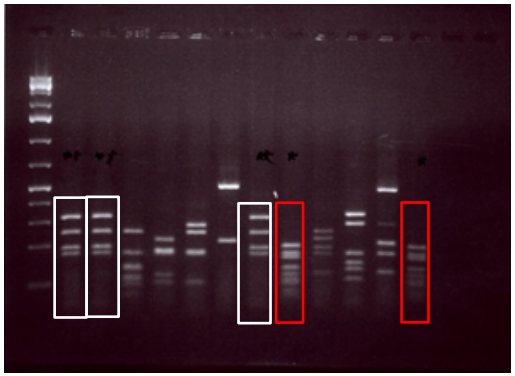

Supplementary Figure S2: Pattern repeats of scFvs (**red** and **white** boxes) generated by panning on (a) GSH-QDs and (b) TiO_2 NPs following a BstNI digest after Round 4 of panning.

Supplementary Figure S3

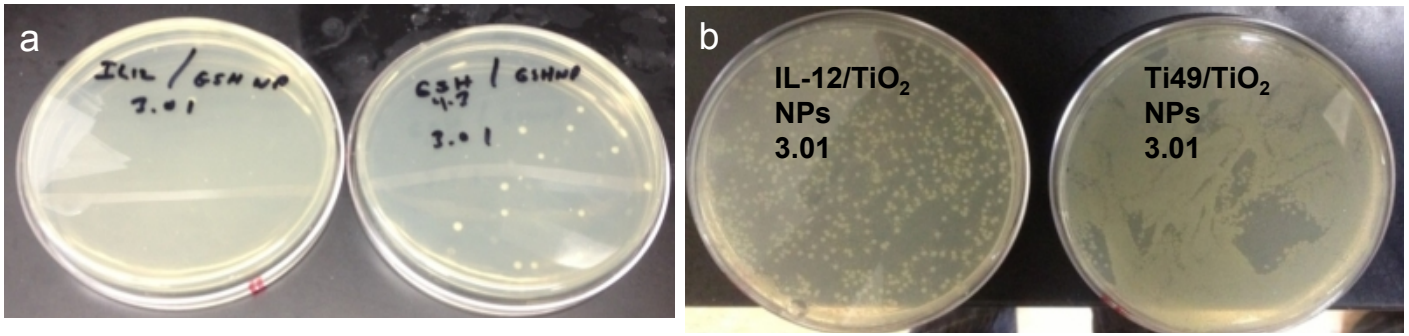

Supplementary Figure S3: **Image of titer plates.** Centrifugation phage titer indicating high binding of phage clone to respective NP target relative to off-target negative control IL-12 phage clone. Plate label indicates Phage clone/NP type and the number indicates phage dilution factor. 3.01 dilution factor indicate 1:1000 of phage diluted in TBS and 10µl was used to infect bacteria cells. **(a)** Phage titer colonies showing ~10-fold more enrichment of GSH43ϕ on GSH-QDs compared to negative control IL-12ϕ on GSH-QDs. **(b)** Phage titer colonies showing ~100-fold more enrichment of Ti49ϕ on TiO2 NP compared to IL-12ϕ on TiO_2 NPs.

Supplementary Figure S4

GSH43ϕ binding GSH-QDs

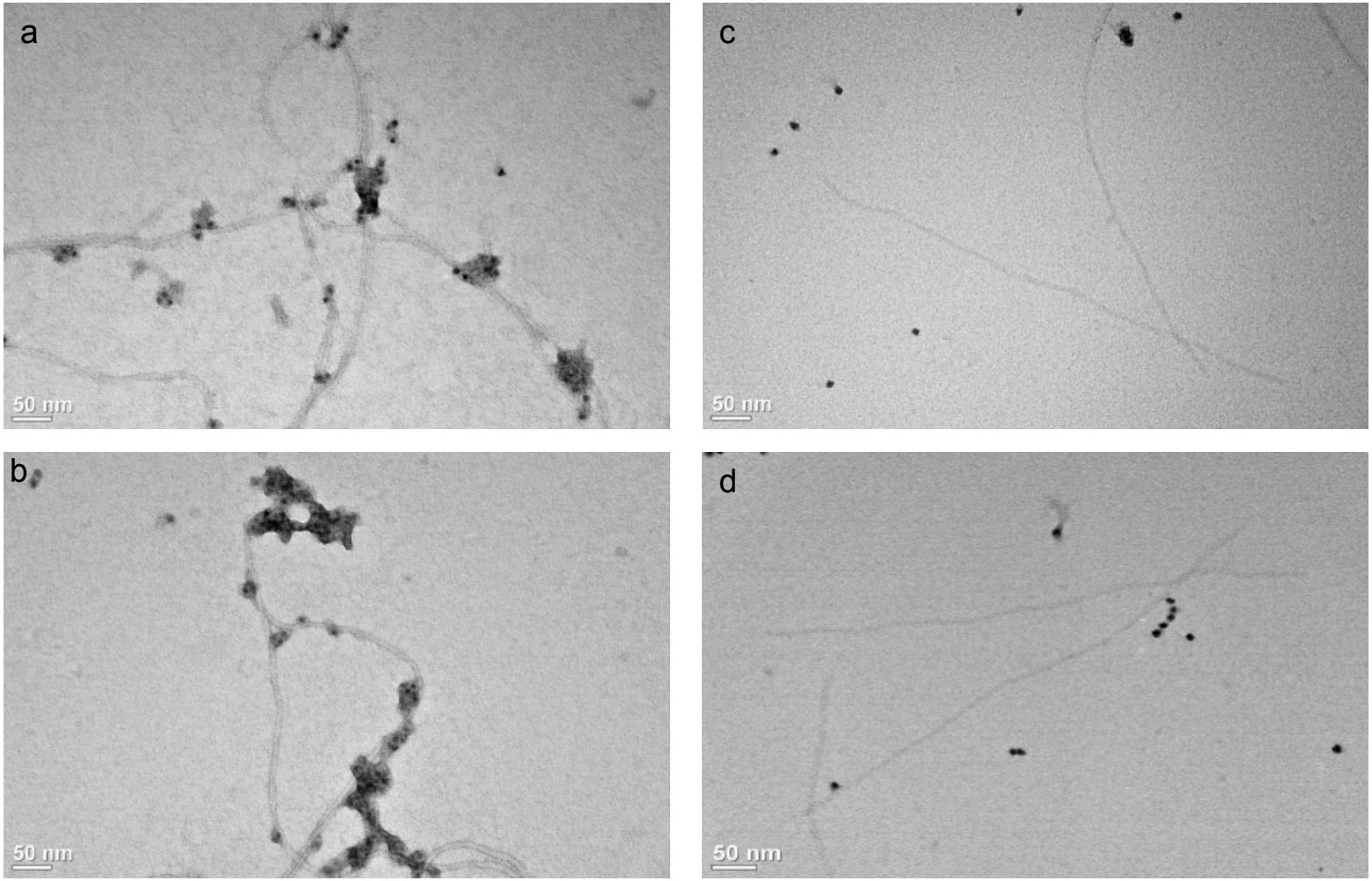

IL12ϕ not binding GSH-QDs

Supplementary Figure S4: Other TEM images of GSH43ϕ and IL12ϕ each mixed separately with GSH-QDs. **(a,b)** GSH43ϕ exhibit strong association and clustering with GSH-QDs whereas **(c,d)** the negative control IL-12ϕ shows no affinity for the GSH-QDs which appear highly dispersed. Scale bar=50 nm.

Supplementary Figure S5

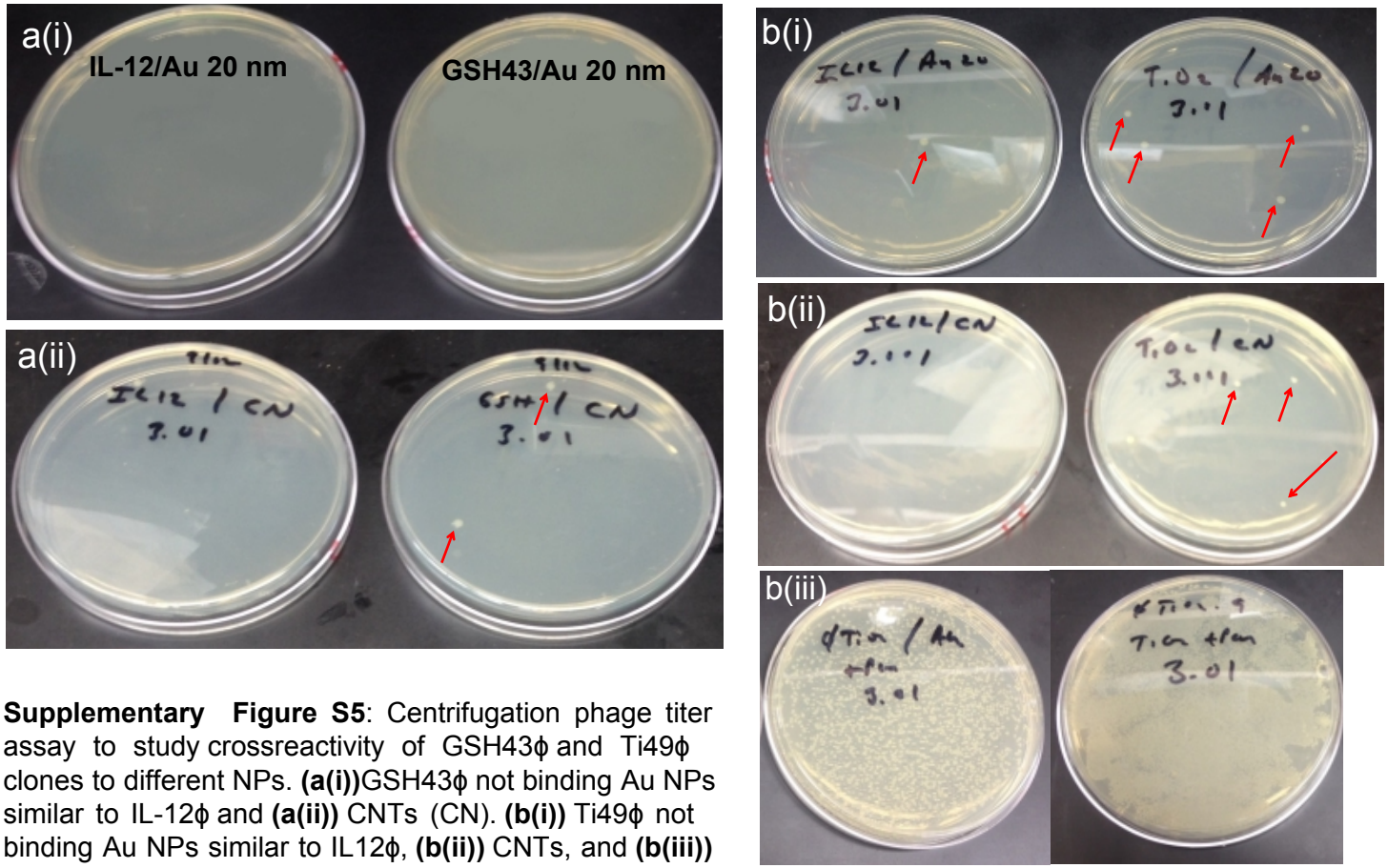

Supplementary Figure S5: Centrifugation phage titer assay to study crossreactivity of GSH43ϕ and Ti49ϕ clones to different NPs. **(a(i))**GSH43ϕ not binding Au NPs similar to IL-12ϕ and **(a(ii))** CNTs (CN). **(b(i))** Ti49ϕ not binding Au NPs similar to IL12ϕ, **(b(ii))** CNTs, and **(b(iii))** Au powder (left) compared to TiO_2 NPs (right) which is more than 100-fold. **Red arrows** indicate colonies not visible clearly. All phage titers were performed at the same dilution (3.01 indicating, 1:1000 phage diluted in TBS and 10 µL used to infect bacterial host cells).

Supplementary Figure S6

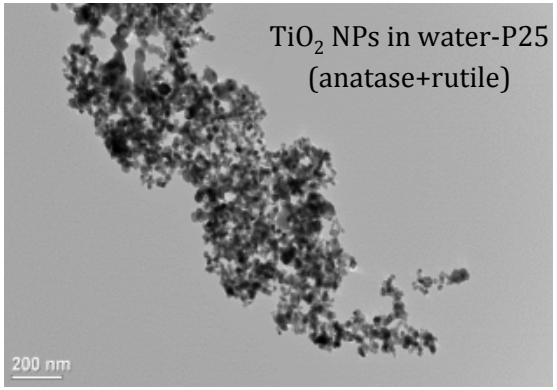

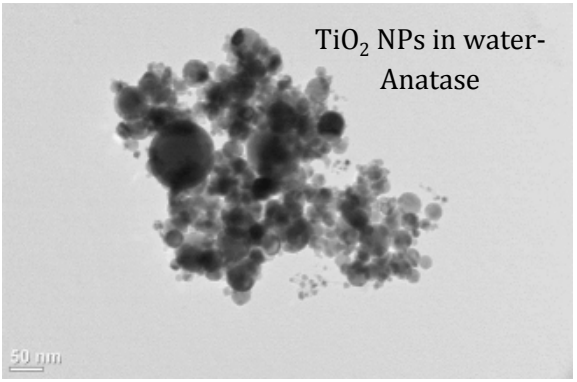

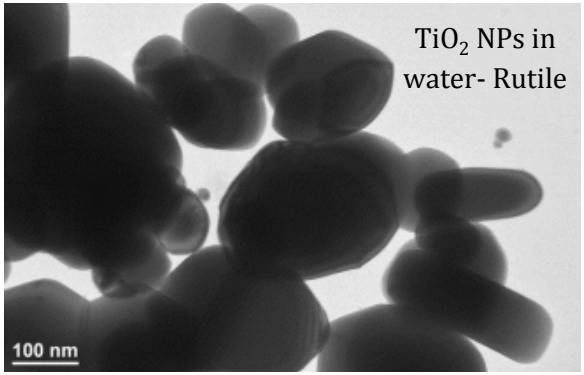

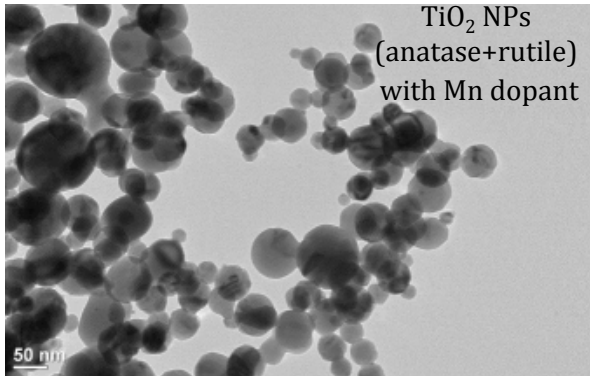

Supplementary Figure S6: TEM Images of TiO_2 NPs. TEM images showing morphology and sizes of various TiO_2 NPs including anatase+rutile (P25), anatase only, rutile only and TiO_2 NPs with 1% Mn as dopant in water. Scale bar= 200, 50, 100, 50 nm respectively.

Supplementary Figure S7

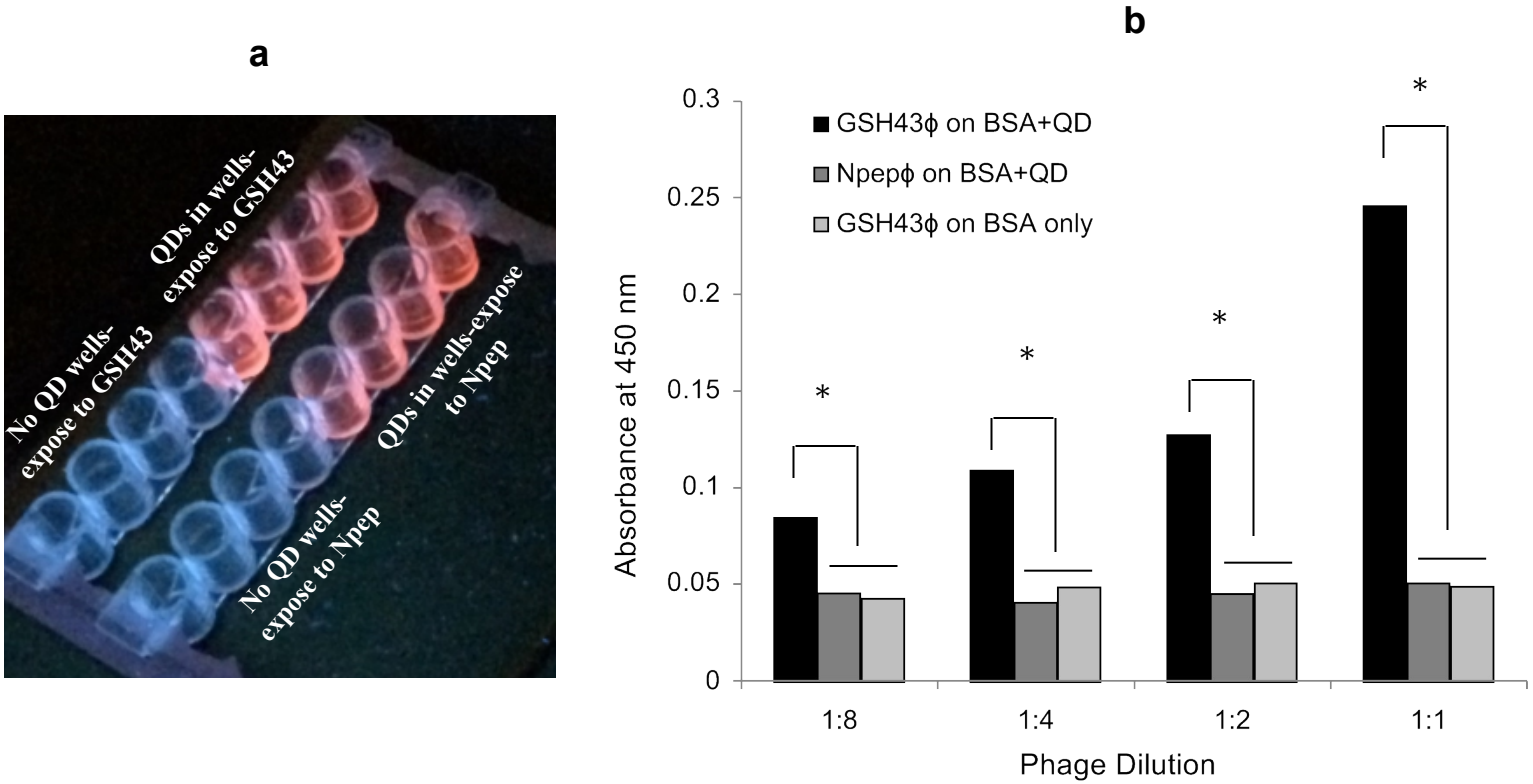

Supplementary Figure S7: **(a)** QDs immobilized on a BSA-coated plated as visible under a UV-lamp whereas wells with no QDs do not fluoresce. **(b)** Phage ELISA assay of GSH43ϕ and negative control (Npepϕ) on QDs immobilized on BSA-coated plates. With an increasing concentration of phage, significantly more binding (*$p<0.05$) of GSH43ϕ to GSH-QDs occurs when detected using TMB substrate at 450 nm, compared to negative control Npepϕ and GSH43ϕ interacting with wells containing BSA alone (no QDs). Values are average of three independent experiments and error bars represent SEM. Statistics was performed using two-tailed unpaired student's t-test.

Supplementary Figure S8

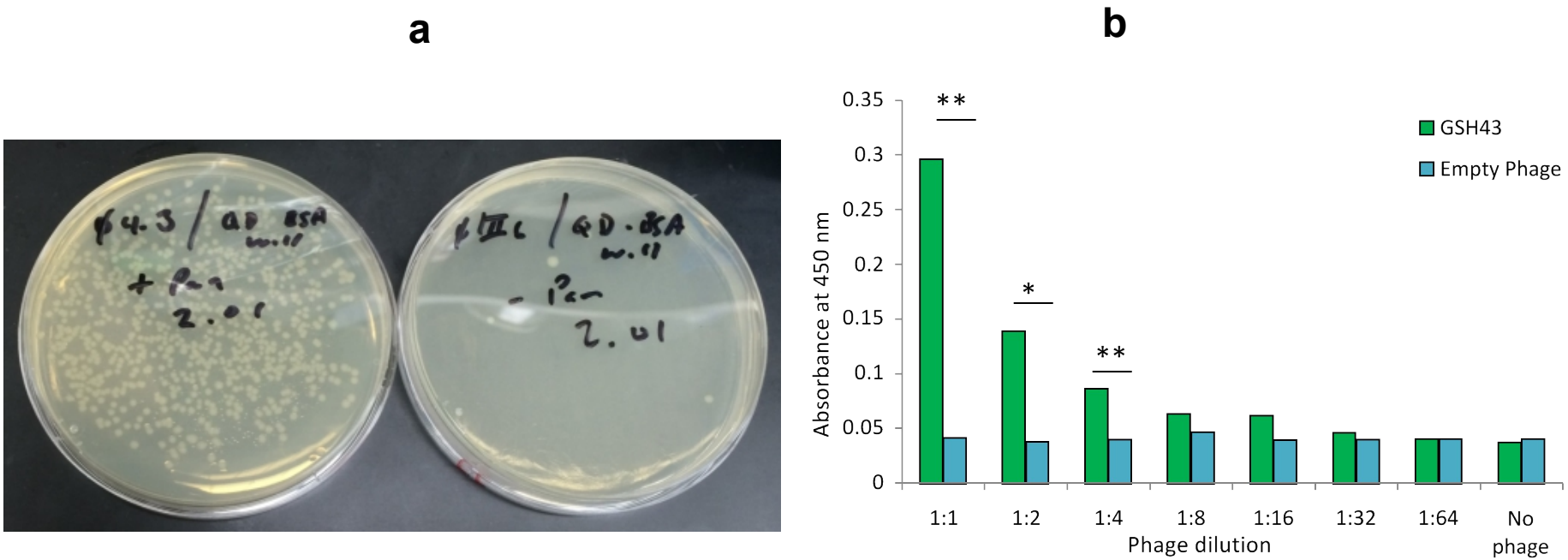

Figure S8: Comparison of GSH43ϕ to empty vector ϕ in binding to GSH-QDs. (a) : Titer images comparing empty vector phage and GSH43ϕ binding GSH-QDs. Plate titer images showing GSH43ϕ (left) exhibiting binding to GSH-QDs (~200-fold) immobilized on BSA, whereas negative control empty phage (not displaying an antibody, right) does not. Labels are of the format phage/target NP and the number indicates dilution. 2.01 represents 1:100 dilution of phage and 10 µL of phage was used to infect TG1 cells **(b)** Plot showing binding of GSH43ϕ relative to empty vector to GSH-coated wells in a phage ELISA assay. GSH43ϕ binds GSH (green bars) significantly over background binding exhibited by negative control empty phage (blue bars). A student's unpaired t-test was used to determine significance, **p<0.01, *p=0.01. Data plotted are average of two independent experiments and error bars represent SEM.

Supplementary Figure S9

a

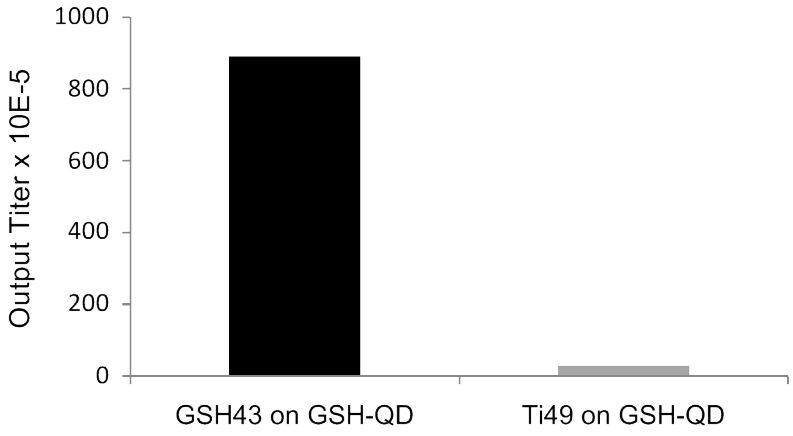

b

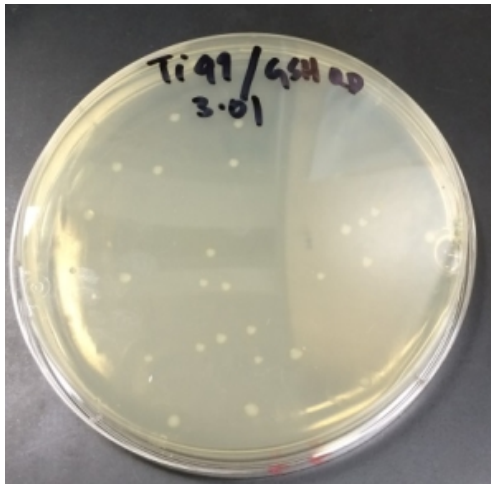

Supplementary Figure S9: Absence of crossreactivity of Ti49 clone to GSH-QDs. (a) Plot showing output titers of GSH43ϕ and Ti49ϕ on GSH-QDs where there is no binding of Ti49ϕ clone to GSH-QDs (~30) compared to GSH43ϕ clone (~900) upon a panning assay where GSH-QDs were immobilized on a BSA coated plate. (b) Image of the plate showing ~30 colonies upon titering the Ti49ϕ on GSH-QDs sample.

Supplementary Figure S10

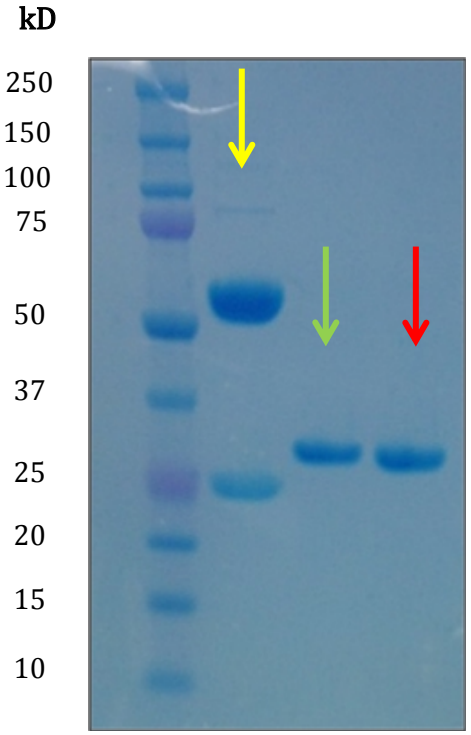

Figure S10: Representative SDS-PAGE Gel. Figure shows presence of purified GSH43-scFv (green arrow) and negative control (NT3-scFv, red arrow)-scFvs indicated by the blue bands (25 kD) compared to a whole antibody control (YerVoy antibody, yellow arrow).

Supplementary Figure S11

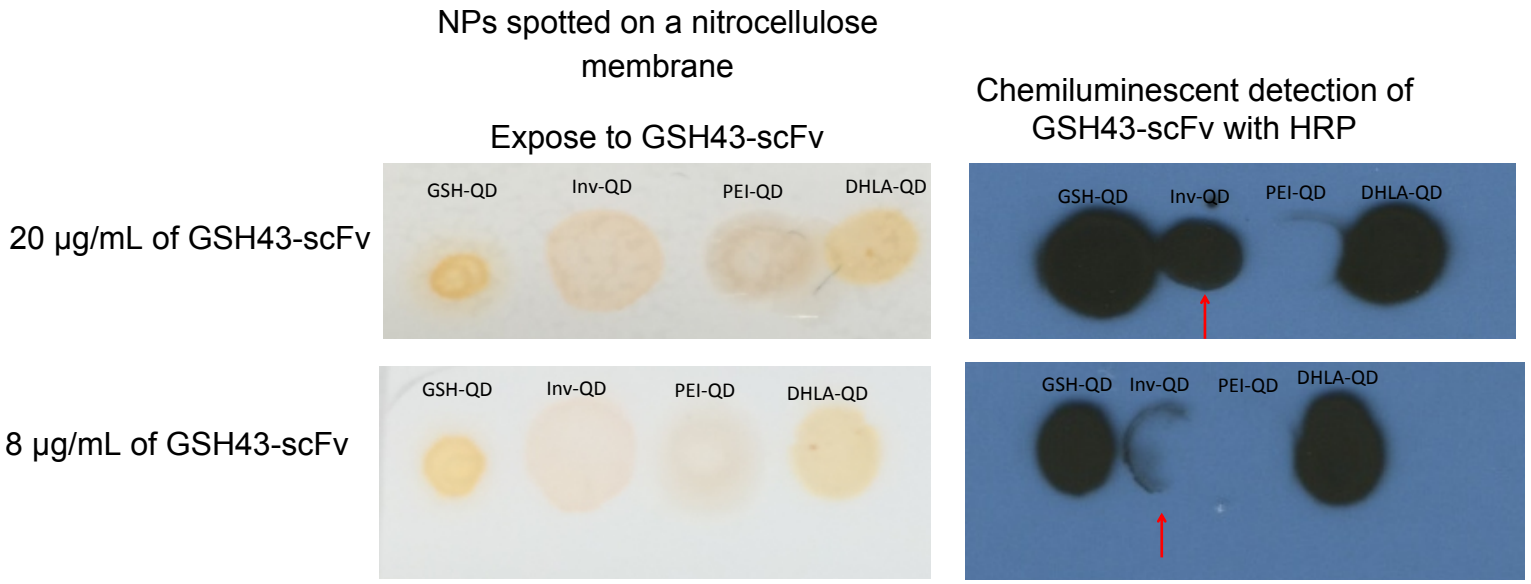

Supplementary Figure S11: Dot blot to verify binding of GSH43-scFvs at different concentrations to Invitrogen ITK™ 565-QDs (Inv-QDs, 1 µL) spotted on a nitrocellulose membrane. GSH43-scFv binds Invitrogen QDs at 20 µg/mL and 8 µg/mL but not 5 µg/mL as discussed in Figure 2. Red arrows detect spot formed upon chemiluminescent detection using HRP indicative of binding to Inv-QDs.

Supplementary Figure S12

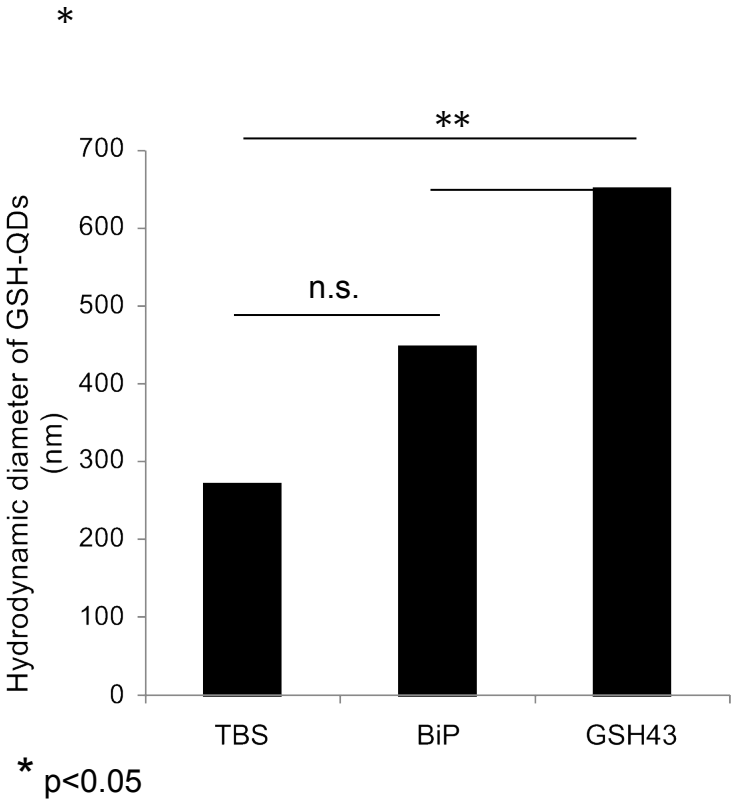

Supplementary Figure S12: Hydrodynamic diameter measurements using the Malvern Zetasizer on GSH-QD mixed 2 hr with BiP or GSH43 scFvs, centrifuged, and resuspended in TBS:water (3:7). GSH43-scfv-QD conjugate shows a significant increase in hydrodynamic diameter compared to BiP-associated QDs ($p<0.05$) and QDs processed in TBS alone ($p<0.01$) using a one-way ANOVA test, whereas BiP-associated complexes do not show any significance (n.s.) compared to QDs in TBS. Error bars indicate SEM of 4 independent experiments.

Supplementary Figure S13

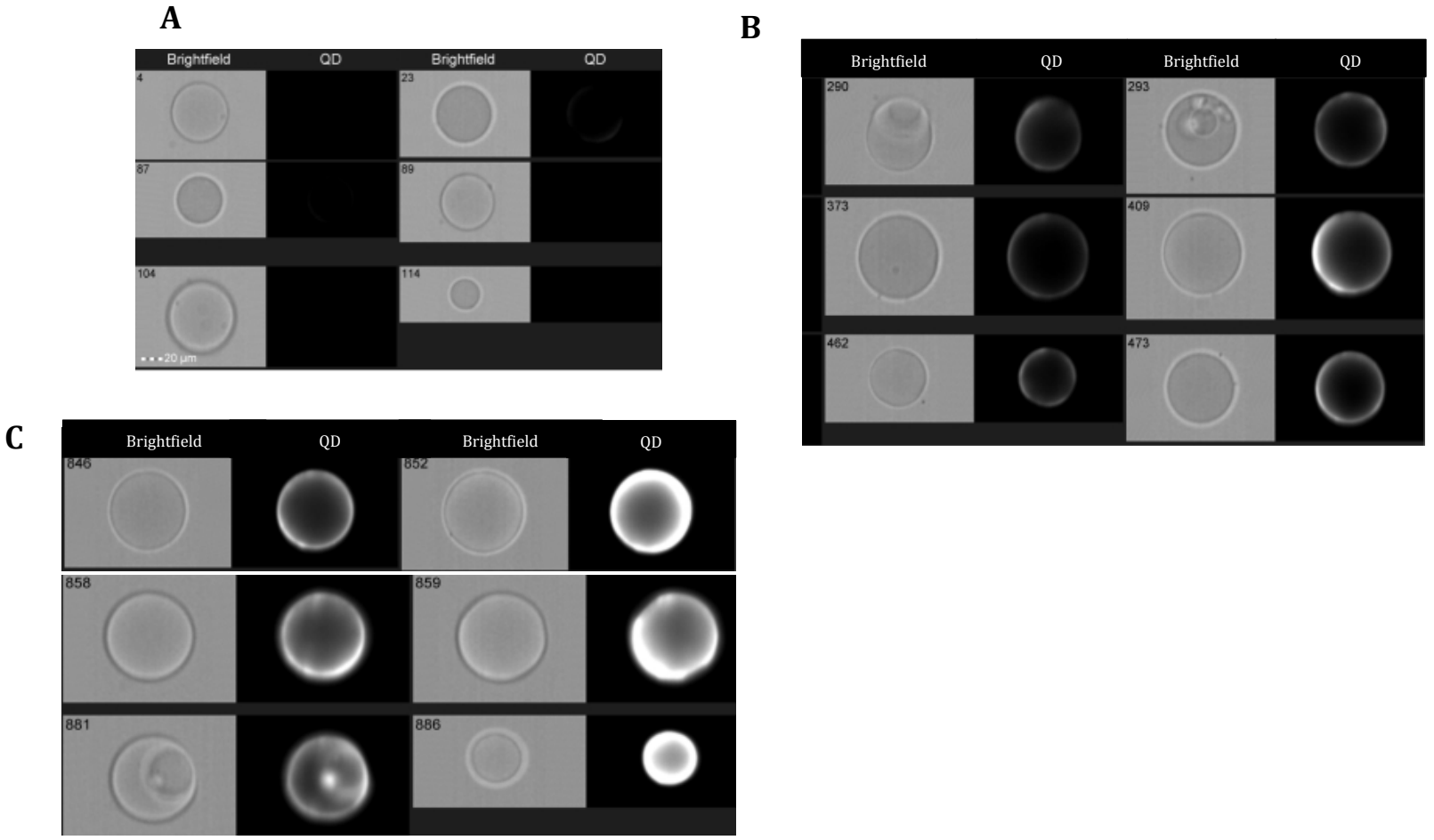

Figure S13: Image Stream Experiment Using Beads. Representative images showing brightfield and QD channels of anti-FLAG coated agarose beads flowing through Image Stream flow cytometer where A) represents beads not coated with scFvs but treated with GSH-QDs. No QD fluorescence is seen in the images indicating that QDs did not nonspecifically bind anti-FLAG coated agarose beads. However, upon coating beads with B) negative control BiP-scFv shows a weak background QD signal is detected however, coating beads with C) GSH43-scFv show intense QD fluorescence exposure indicating the binding of the GSH-QDs to GSH43-scFvs. Scale bar=20 µm.

Supplementary Figure S14

a

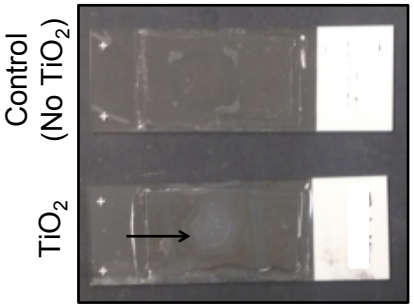

b

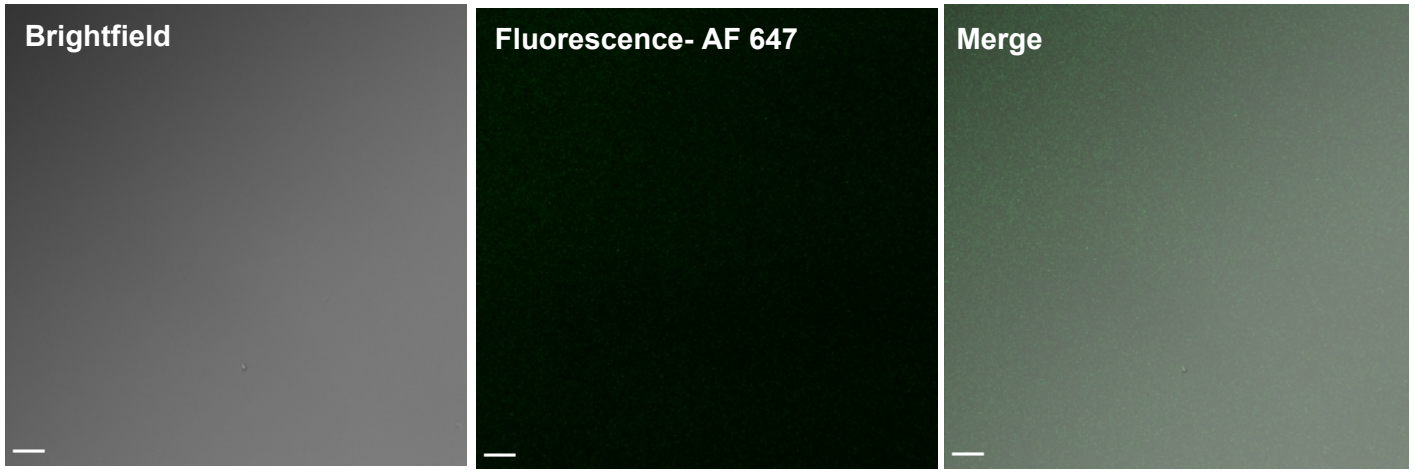

Supplementary Figure S14: **(a)** Slides showing TiO_2 in water dried indicated by the black arrow (**bottom**) whereas control shows no white spot (**top**). **(b)** Confocal images of slide without TiO_2 NPs incubated with Ti49-scFvs followed by detection with Alexa Fluor 647-(pseudo-color **green**) conjugated anti-FLAG antibody. No non-specific staining was observed. Scale bar=20 μm.

Supplementary Figure S15

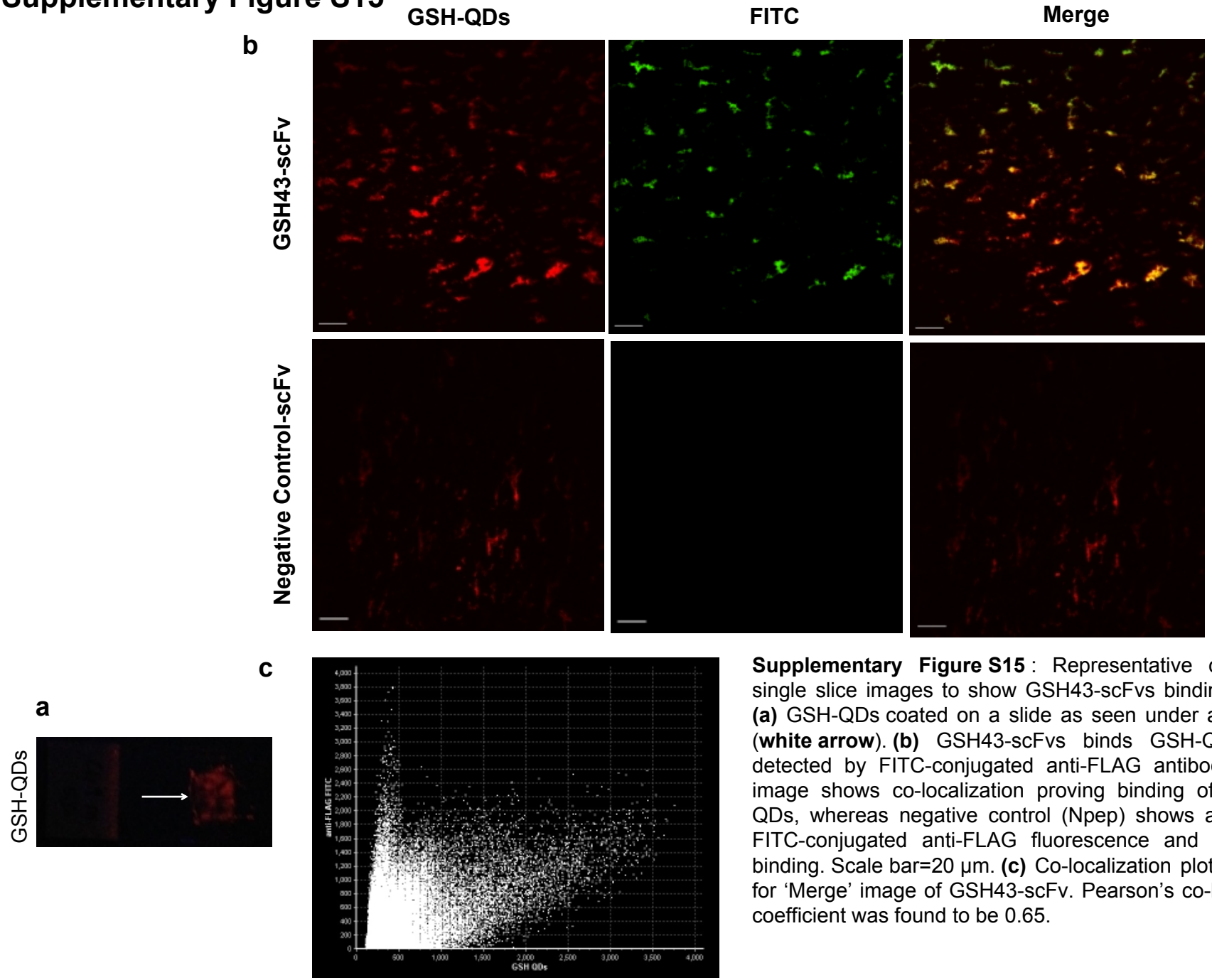

Supplementary Figure S15 : Representative confocal single slice images to show GSH43-scFvs binding to QDs. **(a)** GSH-QDs coated on a slide as seen under a UV lamp (**white arrow**). **(b)** GSH43-scFvs binds GSH-QDs as detected by FITC-conjugated anti-FLAG antibody. Merge image shows co-localization proving binding of scFvs to QDs, whereas negative control (Npep) shows absence of FITC-conjugated anti-FLAG fluorescence and hence no binding. Scale bar=20 µm. **(c)** Co-localization plot obtained for 'Merge' image of GSH43-scFv. Pearson's co-localization coefficient was found to be 0.65.

Supplementary Figure S16

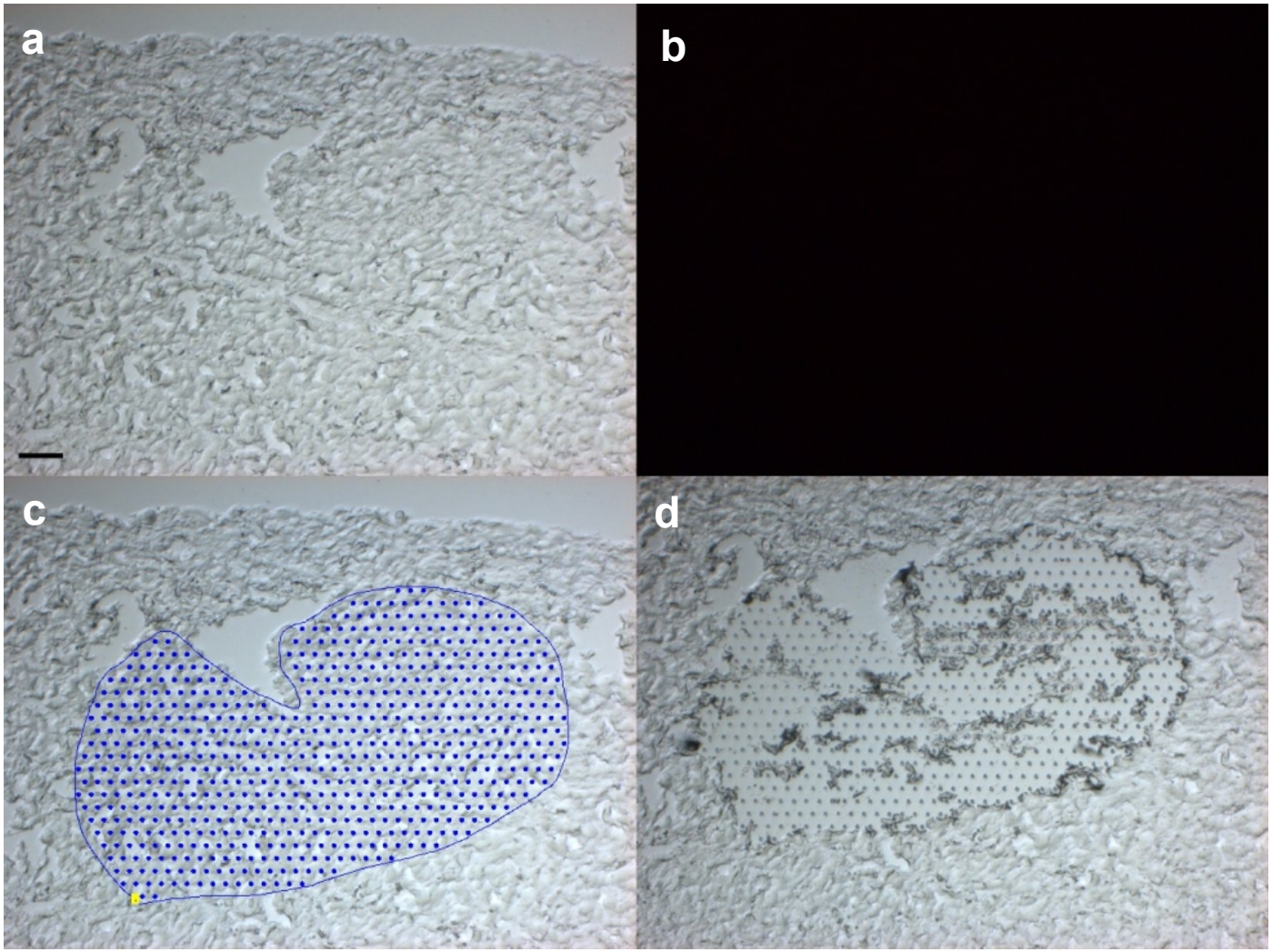

Supplementary Figure S16: LCM imaging of control 'no QD' sample of *ex vivo* human skin. Representative control sample showing **(a)** no AP staining indicating lack of binding of GSH43-scFvs to GSH-QDs. **(b)** Complete absence of GSH-QDs (no fluorescence). **(c)** Portions of tissue sections were marked for cut and captured onto adhesive tube caps using LCM, and processed for AAS. **(d)** The portion of skin remaining after capture is shown. Scale bar=50 µm.

Supplementary Figure S17a

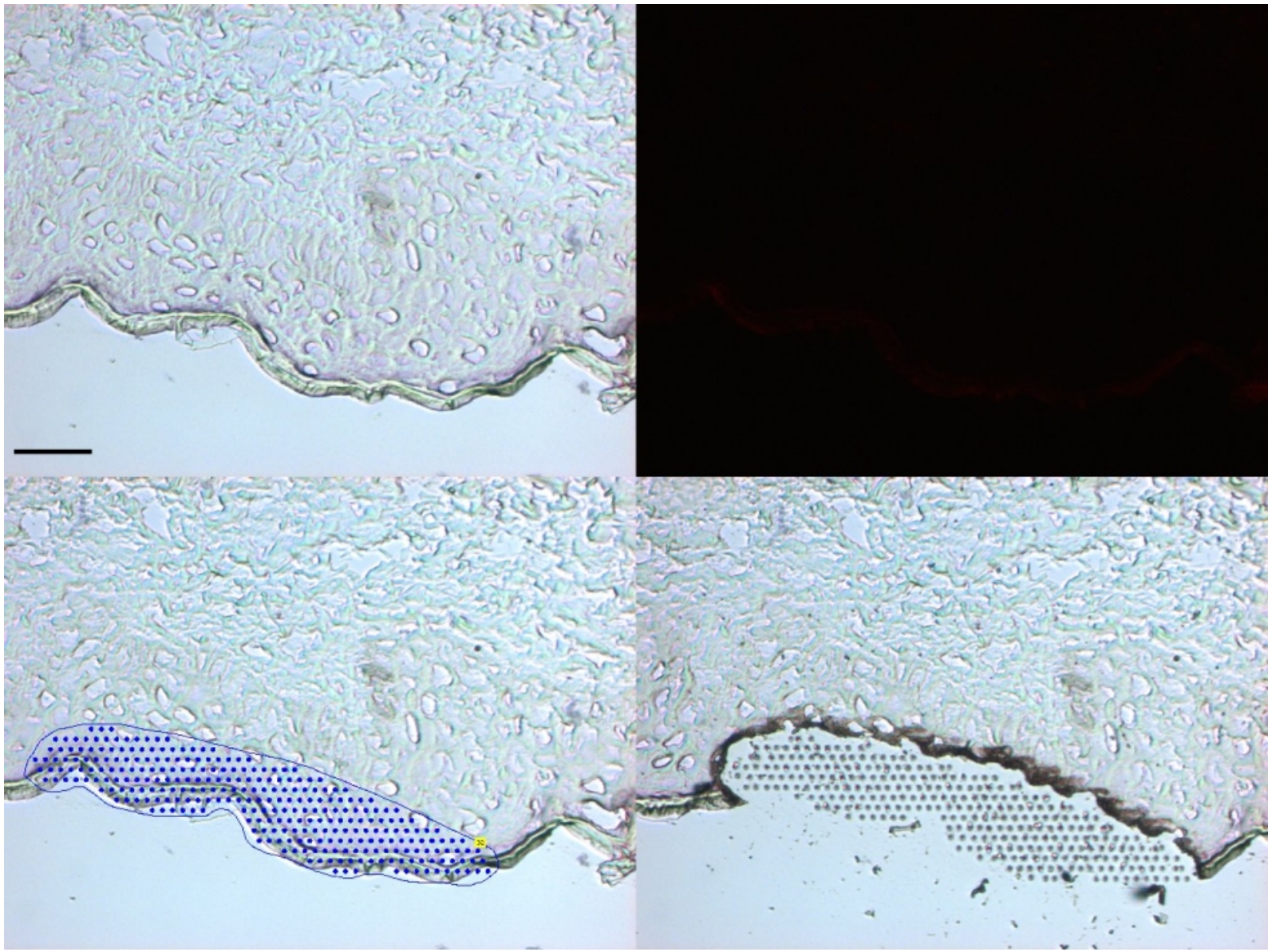

Supplementary Figure S17b

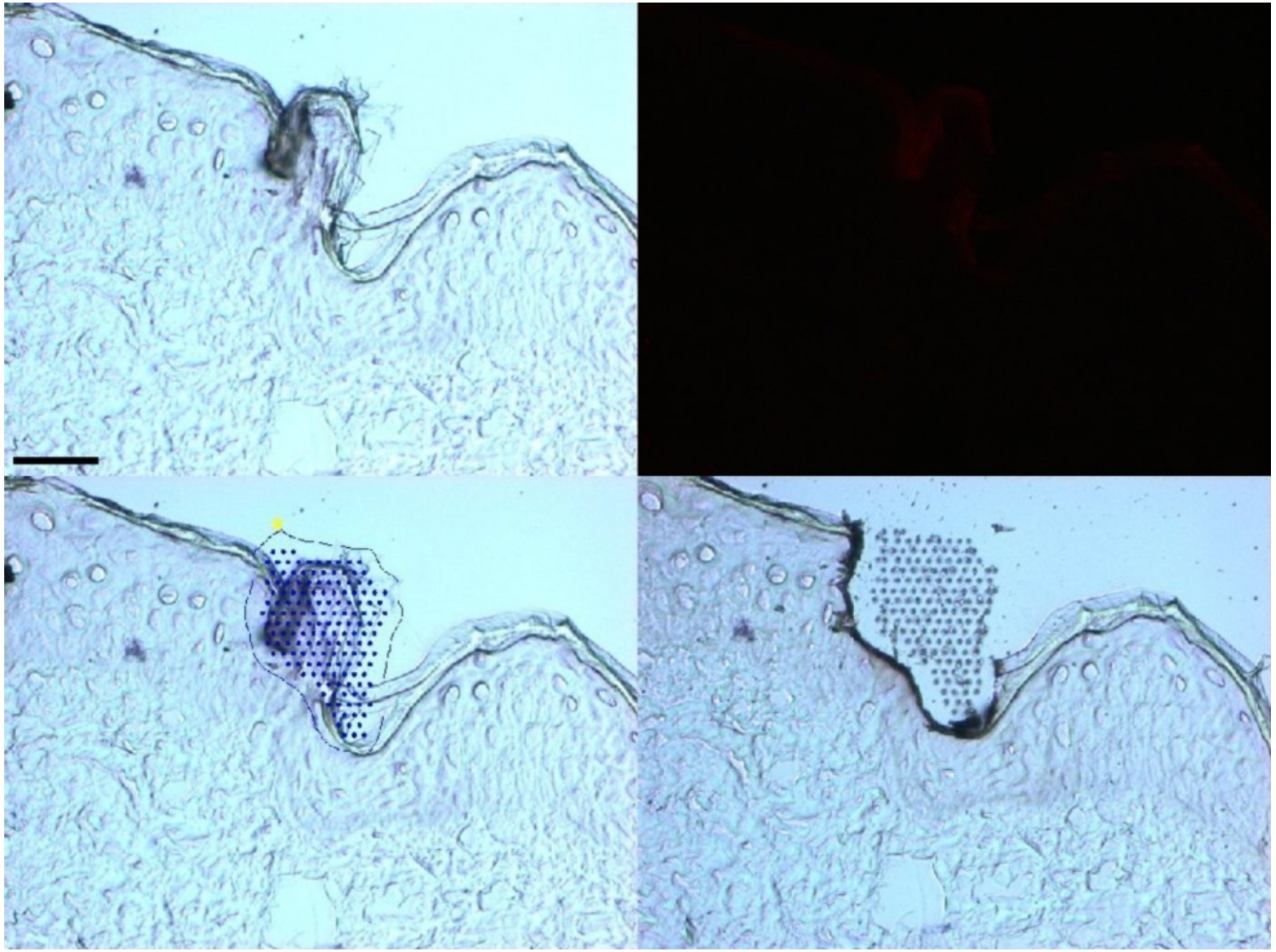

Supplementary Figure S17c

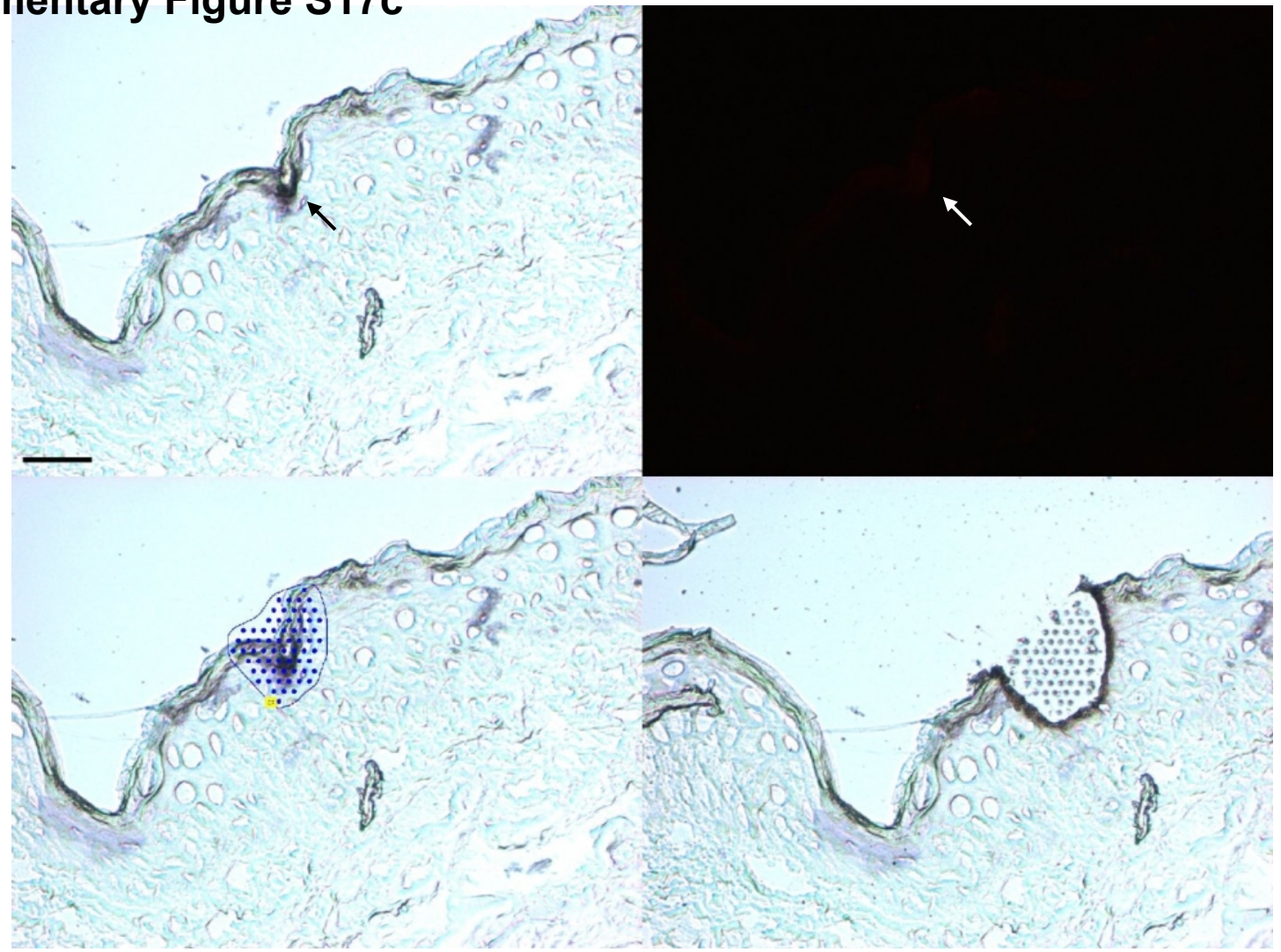

Supplementary Figure S17: Representative images to prove binding of GSH43-scFvs to GSH-QDs applied on epidermis using LCM and AAS. **(a)** Control skin specimen not treated with QDs showing no AP staining in brightfield (**top-left**) and no fluorescence (**top-right**). Upon using LCM to cut and capture (**bottom-left, bottom-right**) portions of skin for AAS analysis, Cd levels (0.0085 ng/mL) were found to be <LOQ (0.025 ng/mL). **(b)** GSH-QDs applied on epidermis shows binding to GSH43-scFvs detected by AP (**top-left**). A portion with visible staining and fluorescence (**top-right**) was marked for cut (**bottom-left**) and captured (**bottom-right**) for AAS analysis. Cd levels were found to be 0.108 ng/mL proving presence of QDs. **(c)** Areas where AP staining was visible (**top-left**) but not fluorescence (**white arrow**, **top-right**), however when samples was marked for cut (**bottom-left)** and captured (**bottom-right**) using LCM, and analyzed using AAS, Cd levels were found to be 0.018 ng/mL which was greater than control. Scale bar=50 µm.

Supplementary Figure S18

a

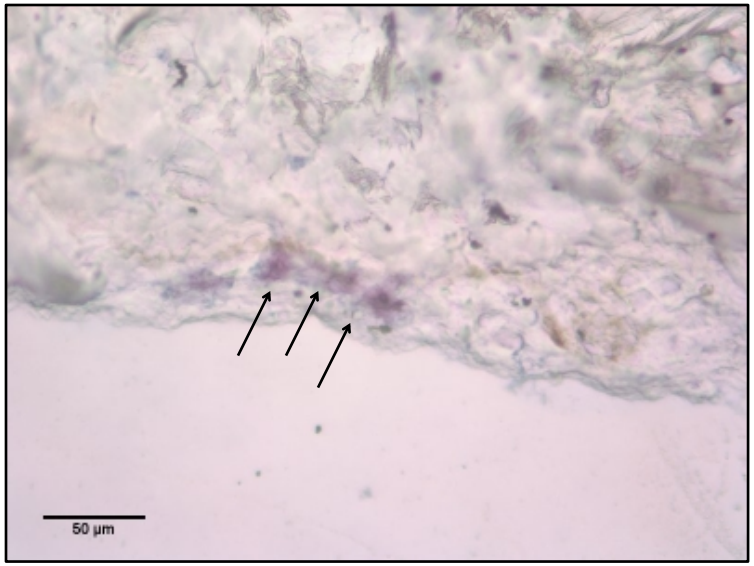

b

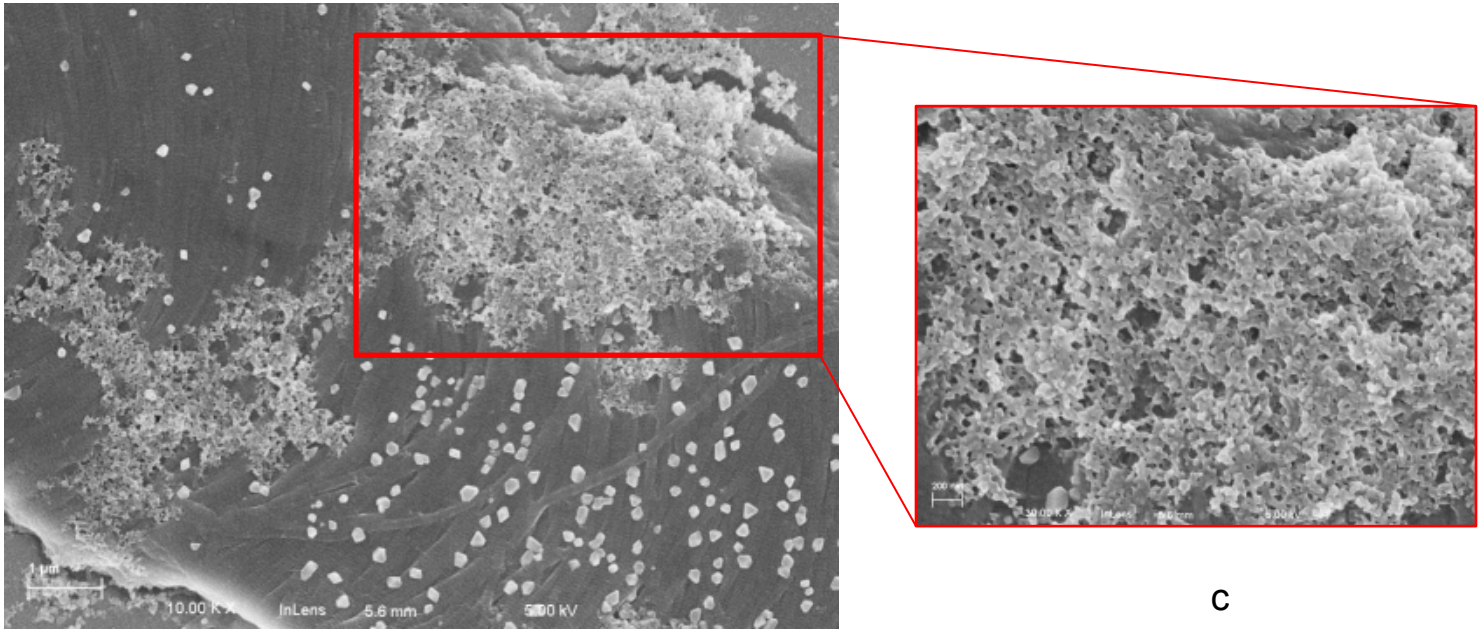

c

Supplementary Figure S18: Positive control human *ex vivo* skin treated with TiO_2 NPs in the dermis of skin. IHC was performed with Ti49-scFvs to prove presence of TiO_2 NPs. (a) Bright-field image showing AP staining (black arrows) with the use of Ti49-scFvs in an *ex vivo* human skin sample upon application of 1 mg/mL TiO_2 NPs in the dermis. (b) SEM image showing TiO_2 NPs and (c) magnified image of the TiO_2 NPs in skin hence proving presence of NPs in the corresponding stained areas.

Supplementary Figure S19

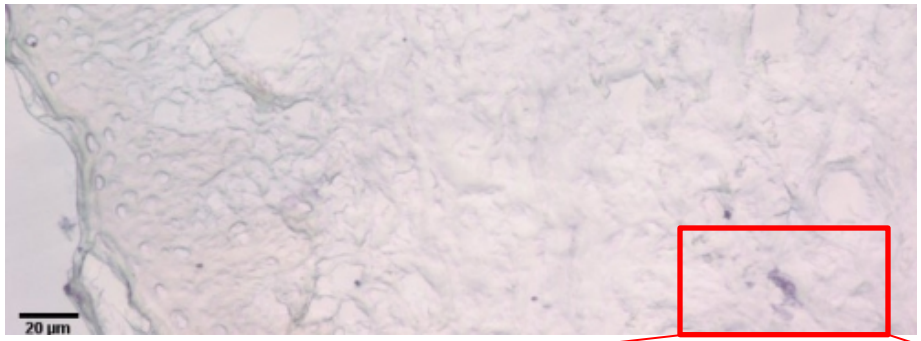

a

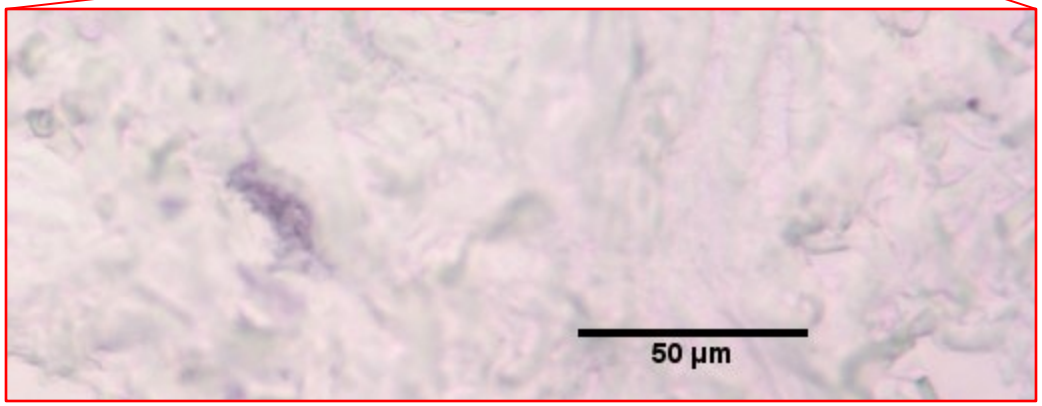

b

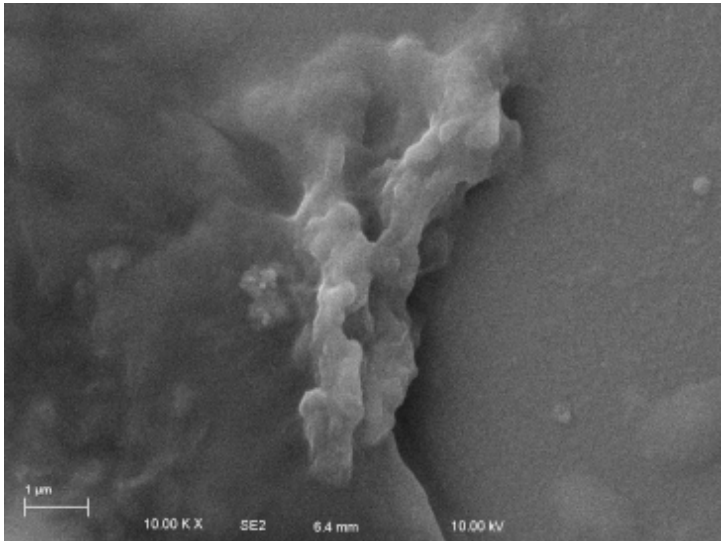

c

Supplementary Figure S19: Tape stripped ex vivo human skin sample treated with TiO_2 NPs showing (a) presence of AP staining in the dermis upon performing IHC with Ti49-scFvs. (b) Examination of the stained area using (c) SEM shows presence of TiO_2 NPs similar in morphology to the TiO2 in the epidermis, Supplementary Figure S17.